OPEN ACCESS

University of Dundee

University of Dundee

An Energy Stable C0 Finite Element Scheme for A Phase-Field Model of Vesicle Motion and Deformation

Shen, Lingyue; Xu, Zhiliang; Lin, Ping; Huang, Huaxiong; Xu, Shixin

Published in:
SIAM Journal on Scientific Computing

DOI:
10.1137/21M1416631

Publication date:
2022

Licence:
CC BY

Document Version
Peer reviewed version

Link to publication in Discovery Research Portal

Citation for published version (APA):
Shen, L., Xu, Z., Lin, P., Huang, H., & Xu, S. (2022). An Energy Stable C^0 Finite Element Scheme for A Phase-Field Model of Vesicle Motion and Deformation. *SIAM Journal on Scientific Computing*, *44*(1), B122-B145. https://doi.org/10.1137/21M1416631

General rights
Copyright and moral rights for the publications made accessible in Discovery Research Portal are retained by the authors and/or other copyright owners and it is a condition of accessing publications that users recognise and abide by the legal requirements associated with these rights.

- Users may download and print one copy of any publication from Discovery Research Portal for the purpose of private study or research.
- You may not further distribute the material or use it for any profit-making activity or commercial gain.
- You may freely distribute the URL identifying the publication in the public portal.

Take down policy
If you believe that this document breaches copyright please contact us providing details, and we will remove access to the work immediately and investigate your claim.

Download date: 29. Jun. 2022

An Energy Stable C^0 Finite Element Scheme for A Phase-Field Model of Vesicle Motion and Deformation

Lingyue Shen[1], Zhiliang Xu[6], Ping Lin[1], Huaxiong Huang[3,4,5], and Shixin Xu*[2]

[1]*Department of Mathematics University of Dundee Dundee DD1 4HN*
[2]*Duke Kunshan University, 8 Kunshan Street, Kunshan, Jiangsu, China*
[3]*Research Centre for Mathematics, Advanced Institute of Natural Sciences, Beijing Normal University (Zhuhai), China;*
[4]*BNU- HKBU United International College, Zhuhai, China*
[5]*Department of Mathematics and Statistics,York University, 4700 Keele Street Toronto, Ontario CANADA M3J 1P3*
[6]*Department of Applied and Computational Mathematics and Statistics, University of Notre Dame,102G Crowley Hall, Notre Dame, IN 46556*

DEC,20,2021

Abstract

A thermodynamically consistent phase-field model is introduced for simulating motion and shape transformation of vesicles under flow conditions. In particular, a general slip boundary condition is used to describe the interaction between vesicles and the wall of the fluid domain. A second-order accurate in both space and time C^0 finite element method is proposed to solve the model governing equations. Various numerical tests confirm the convergence, energy stability, and conservation of mass and surface area of cells of the proposed scheme. Vesicles with different mechanical properties are also used to explain the pathological risk for patients with sickle cell disease.

Keywords— Vesicle; Local inextensibility; Energy stable scheme; Narrow channel.

1 Introduction

Studying dynamic motion and shape transformation of biological cells is always a point of interest in cell biology, because the shapes of the cells usually relate to their function. For example, many blood-related diseases are known to be associated with alterations in the geometry and membrane properties of red blood cells [64]. Red blood cells in diabetes or sepsis patients exhibit impaired cell deformability [22, 50]. During blood clot formation, an indicator of platelet activation is its shape change by forming filopodia and lamellipodia. Notably, platelets shape changes facilitate their adhesion to the site of vascular injury and cohesion with other platelets or erythrocytes [62, 2].

© 2022. This manuscript version is made available under the CC-BY 4.0 license http://creativecommons.org/licenses/by/4.0/

In *in silico* study, it is vitally important to establish a proper model [41, 8, 15, 46] of cell membranes for analyzing the dynamical shape transformation of cells in addition to modeling intracellular and extracellular fluids. Various mathematical models were introduced for predicting cell morphology and function. Dissipative particle dynamics (DPD) [39] models of red blood cell were developed in [49, 39, 48], and were used to study effects of red blood cells on platelet aggregation [49]. Models based on interface tracking or capturing such as level set method [70, 69, 58] were also developed [7, 35, 31, 30] to take into consideration the fluid-cell-structure interaction. In numerical treatment, various methods such as immersed boundary method [36, 60, 47, 65, 68], immersed interface method [32, 37], and fictitious domain method [30] using finite difference or finite element formulation have been introduced to solve governing equations of these models.

Recently the phase-field approach has become one of the popular choices for modeling complicated evolution of various structures presented in biological problems [19, 8, 41] as well as problems in other scientific disciplines [40, 13, 66, 71]. The phase-field method considers the material interface as a diffuse layer instead of a sharp discontinuity. This regularization can be rigorously formulated through a variational process. The main advantages of the phase-field method are twofolds. The phase-field order parameter identifying the diffuse interface is treated as an additional primary unknown of the problem to be solved on the whole domain. Consequently, interface transformations are predicted without the necessity of a remeshing algorithm to treat the evolution of the interface. The physics mediating the interface dynamics can be easily incorporated into the phase-field models.

Lots of phase-field type vesicle models have been introduced lately [33, 79, 42, 17, 14, 18, 6, 80, 9, 67] . Mechanical properties of the vesicle membrane such as bending stiffness and inextensibility can be modeled rigorously by the phase-field theory [17, 15, 16, 19] to establish a more comprehensive model. For instance, the bending energy $E_{elastic}$ of bending resistance of the lipid bilayer membrane Γ in the isotropic case (neglecting the proteins and channels on the membrane) given in the form of the Helfrich bending energy

$$E_{elastic} = \int_{\Gamma} \frac{k}{2} H^2 ds \ , \tag{1}$$

can be approximated by a modified elastic energy defined on the whole domain in the phase-field formulation [12, 18, 15, 16]. Here k is the bending modulus and H is the mean curvature of the membrane. Constraints conserving cell mass and ensuring global inextensibility of cell membrane are frequently introduced into vesicle models to keep the mass and surface area of the vesicle constant [19, 1].

The focus of this paper is to model flowing vesicles interacting with the domain boundaries which mimics scenarios such as red blood cells passing a narrowed blood vessel. This involves considering a moving contact line problem. The first goal of this paper thus is to derive a thermodynamically consistent phase-field model for vesicles' motion and shape transformation in a closed spatial domain by using an energy variational method [61, 72, 74, 27]. All the physics taken into consideration are introduced through definitions of energy functionals and dissipation functional, together with the kinematic assumptions of laws of conservation. Besides the energy and dissipation terms defined on the bulk region of the domain, terms accounting for boundary effects are also added to the functionals. Then performing variation of these functionals yields an Allen-Cahn-Navier-Stokes (ACNS) system [67] with Allen-Cahn general Navier boundary conditions (GNBC) [52]. This is in contrast to most previous works [15, 16, 9] in which dynamic boundary condition was rarely derived during the course of model derivation. Dirichlet or Neumann type conditions were simply

added to these models at the end to close the governing equations [1, 19, 18]. Moreover, in our model derivation, the incompressibility of the fluid, the local and global inextensibility of the vesicle membrane and the conservation of vesicle mass are taken into account by introducing two Lagrangian multipliers, hydrostatic pressure p and surface pressure λ [47] and penalty terms, respectively.

The second goal of this paper is to propose an efficient and accurate numerical scheme for solving the obtained fourth-order nonlinear coupled partial differential equation (PDE) system. Over the past decades, a lot of schemes have been developed for Allen-Cahn- or Cahn-Hilliard-Navier-Stokes systems [8, 11, 76, 13, 10, 28, 78, 77]. As for systems such as vesicle models introduced in the current and other works which are more sophisticated than Allen-Cahn- or Cahn-Hilliard-Navier-Stokes systems, backward Euler time discretization method is frequently used [1, 15, 24, 23] leading to a first-order accurate scheme. Later on, decoupled energy stable schemes are proposal by Chen & Yang in [9], and Francisco & Giordano [25] by introducing explicit, convective velocities. In the current work, an efficient, energy-law preserving (thus energy stable) and second-order accurate C^0 finite element (FE) scheme is proposed to solve the obtained vesicle system using ideas introduced in [28]. The key idea of this scheme is to utilize the mid-point method in time discretizaiton to ensure the accuracy in time, and the form of the law of the discrete energy dissipation is same as that of the continuous model. In order to properly treat the term related to inextensibility of the membrane, a relaxation term of local inextensibility as in [1] is introduced. The numerical study of convergence confirms the proposed scheme is second-order convergence in both time and space. Furthermore vesicle deformation simulations illustrate it is energy stable, and numerically conserves mass and surface area of vesicles.

The introduction of the GNBC in this work makes it possible to study the more complicated fluid-structure interaction problems. In this paper, the developed model is applied to studying vesicles passing narrow channels. The results confirm that the more rounded the vesicles (smaller surface-volume ratio) are, the more likely the vesicles form lockage when they pass through narrow channels. It is also worth noting that it is critical to include the local inextensibility of the vesicle membrane in the model when studying this type of problems. Without the local inextensibility, the vesicle membrane can be falsely stretched or compressed. Lastly, although membrane structures of vesicles and blood cells are quite different, a blood cell in many studies can be treated as an elastic capsule with bending rigidity, in which the membrane is impenetrable to both interior and exterior fluids. Therefore our model developed for vesicles can be readily applied for studying a vast body of blood cells related problems [44].

The rest of paper is organized as follows. Section 2 of the paper begins with introducing basic dynamical assumptions that have been used in many papers [19, 51], and is devoted to model derivation. Dimensionless model governing equations and the energy decaying law of the model are presented in Section 3. In Section 4, the numerical scheme solving the proposed model is developed, and its energy law is given. Numerical simulation results are described in Section 5 to confirm the energy law of the numerical scheme and the feasibility of our model. A case study of vesicle passing through a narrow channel is shown, which is to simulate the motion of red blood cells in blood vessel. Conclusions are drawn in Section 6.

2 Model Derivation

Derivation of the model for simulating a flowing vesicle deforming in a channel filled with extracellular fluid is presented in this section. The phase-field label function ϕ is introduced to track the motion of the vesicle, where $\phi(\boldsymbol{x}) = \pm 1$ denotes the intracellular and extracellular space, and $\phi = 0$ is the vesicle membrane or interface.

The model is derived using an energy variational method [61]. It begins with defining two functionals, namely, the total energy and dissipation of the system, and introducing the kinematic equations based on physical laws of conservation. The specific forms of the fluxes and stresses in the kinematic equations are obtained by taking the time derivative of the total energetic functional and comparing with the defined dissipation functional. More details of this method can be found in [61, 74].

In what follows, we detail steps of using this method to derive the model. We first make the following assumptions about mass and momentum conservation of the mixture of extracellular fluid and vesicle and the interface inextensibility, and assume that the dynamics of the phase field function ϕ follows an L^2 gradient flow:

$$\begin{cases} \frac{\partial \phi}{\partial t} + \nabla \cdot (\mathbf{u}\phi) = q_\phi \ , \\ \rho(\frac{\partial \mathbf{u}}{\partial t} + (\mathbf{u} \cdot \nabla)\mathbf{u}) = \nabla \cdot \boldsymbol{\sigma}_\eta + \mathbf{F}_\phi \ , \\ \nabla \cdot \mathbf{u} = 0 \ , \\ \delta_\gamma(\mathcal{P} : \nabla \mathbf{u}) = 0 \ . \end{cases} \tag{2}$$

with forms of flux q_ϕ, stress $\boldsymbol{\sigma}_\eta$ and body force density $\boldsymbol{F}_\phi$ to be determined. Here ρ and $\mathbf{u}$ are the density and velocity of the mixture, respectively. The first equation is the Allen-Cahn type equation to track the interface. The second equation is the conservation of momentum. The third equation accounts for the fluid incompressibility (or mass conservation).

The last equation is related to the local inextensibility of the vesicle membrane which prevents from stretching on any point of the vesicle membrane surface [5]. In the sharp interface model, the local inextensibility (or mass conservation on the interface) is represented by $\nabla_\Gamma \cdot \mathbf{u} = 0$ defined on the interface Γ [42, 44]. This equation is equivalent to $\mathcal{P} : \nabla \mathbf{u} = 0$ where the projection operator $\mathcal{P}$ is defined to be $(I - \mathbf{n}_m \otimes \mathbf{n}_m)$, and $\mathbf{n}_m = \frac{\nabla \phi}{|\nabla \phi|}$ is the unit outward normal vector of the interface when it is defined as an implicit surface by the level function. In the phase-field formulation, the interface is modelled as a diffuse layer. This is different from the sharp interface concept. For computational convenience using phase-field formulation, this local inextensibility constraint on the interface Γ is extended to the domain Ω by multiplying with a scalar function

$$\delta_\gamma = \frac{1}{2}\gamma^2 |\nabla \phi|^2 \ , \tag{3}$$

where $\nabla \phi$ is nonzero only in the diffuse interface layer, and γ is related to the thickness of the diffuse interface layer.

On the wall boundary $\partial \Omega_w$ of the domain, the following boundary conditions are assumed

$$\begin{cases} \mathbf{u} \cdot \mathbf{n} = 0 \ , \\ \mathbf{u}_\tau \cdot \boldsymbol{\tau}_i = f_{\tau_i} \ , \\ \dot{\phi} = \frac{\partial \phi}{\partial t} + \mathbf{u} \cdot \nabla_\Gamma \phi = J_\Gamma \ , \\ f = 0 \ , \\ \partial_n \lambda = 0 \ , \end{cases} \tag{4}$$

where an Allen-Cahn type boundary condition is employed for ϕ, $\mathbf{u}_\tau = \mathbf{u} - (\mathbf{u}\cdot\mathbf{n})\mathbf{n}$ is the fluid slip velocity with respect to the wall, $\boldsymbol{\tau}_i, i = 1, 2$ are the tangential directions on the wall surface (2D), and $\nabla_\Gamma = \nabla - \mathbf{n}(\mathbf{n}\cdot\nabla)$ is the surface gradient operator on the boundary $\partial\Omega_w$. Here the subscript Γ refers to $\partial\Omega_w$, and $\mathbf{n}$ is its unit outward normal. The meaning of equation $f = 0$ will be explicit after definition of the interface curvature (see Eq. (8)). λ, $\partial_n\lambda$, J_Γ are not defined.

The rest part of this section is devoted to deriving the exact forms of q_ϕ, $\boldsymbol{\sigma}_\eta$, $\mathbf{F}_\phi$ and J_Γ using the energy variational method [61, 74]. By following the works in [67, 17], the total energy functional E_{total} of a cell- (or vesicle-) fluid system is defined to be the sum of the kinetic energy E_{kin}, the cell membrane energy E_{cell} and the specific wall energy E_w due to the cell-wall interaction

$$E_{total} = \underbrace{E_{kin}}_{Macroscale} + \underbrace{E_{cell} + E_w}_{Microscale} . \tag{5}$$

The kinetic energy accounts for the transport of the cell-fluid mixture, and is defined as:

$$E_{kin} = \int_\Omega \left(\frac{1}{2}\rho|\mathbf{u}|^2\right) d\boldsymbol{x} , \tag{6}$$

where ρ is the macroscale density of the mixture, and is assumed to be equal to a constant ρ_0 in this work (matched density case).

The cell energy E_{cell} is defined to be the sum of the bending energy $E_{bending}$ and two penalty terms in order to preserve the total volume and surface area of the cell,

$$E_{cell} = E_{bend} + \frac{M_v}{2}\frac{(V(\phi) - V(\phi_0))^2}{V(\phi_0)} + \frac{M_s}{2}\frac{(S(\phi) - S(\phi_0))^2}{S(\phi_0)} , \tag{7}$$

where $V(\phi) = \int_\Omega \phi d\boldsymbol{x}$ is the volume difference of the cell-fluid system and the value of $S(\phi) = \int_\Omega \frac{G(\phi)}{\gamma} d\boldsymbol{x}$ is used to measure the surface area of the cell. M_v and M_s are cell volume and surface area constraint coefficients, respectively.

If the cell membrane is assumed to be isotropic and only composed of lipid bilayer, the bending energy of the bending resistance of the cell membrane can be modeled by the Helfrich bending energy [17]. If we let $G(\phi) = \int_\Omega \frac{\gamma^2|\nabla\phi|^2}{2} + \frac{(1-\phi^2)^2}{4} d\boldsymbol{x}$ be the free energy of the membrane surface, the curvature of membrane can be calculated as

$$f(\phi) := \frac{\delta G}{\delta \phi} = -\gamma^2\Delta\phi + (\phi^2 - 1)\phi . \tag{8}$$

Then the Helfrich bending energy can be regularized as follows

$$E_{bend} = \int_\Omega \frac{\hat{\kappa}_B}{2\gamma}\left|\frac{f(\phi)}{\gamma}\right|^2 d\boldsymbol{x} , \tag{9}$$

where $\hat{\kappa}_B$ is the bending modulus.

In order to account for the interaction between vesicle and the channel wall $\partial\Omega_w$, when the vesicle passes through the fluid flow channel, the wall free energy E_w is introduced

$$E_w = \int_{\partial\Omega_w} f_w(\phi) ds , \tag{10}$$

where f_w is the vesicle-wall interaction energy density. Here we borrow the idea introduced in moving contact lines models [53, 51] to account for hydrophobic or hydrophilic property of the channel wall

$$f_w(\phi) = -\frac{\sigma}{2}\sin\left(\frac{\phi\pi}{2}\right)\cos(\theta_s)\ , \tag{11}$$

with the static contact angle θ_s [56, 55]. When θ_s is an acute angle, it means there is adhesion force between vesicles and walls. The term $\sin(\frac{\phi\pi}{2})$ is a smooth interpolation between $\pm\frac{\sigma}{2}$.

The chemical potential μ is obtained by taking the variation of $E_{bulk} = E_{kin} + E_{cell}$ with respect to ϕ,

$$\mu = \frac{\delta E_{bulk}}{\delta\phi} = \frac{\hat{\kappa}_B}{\gamma^3}g(\phi) + M_v\frac{V(\phi)-V(\phi_0)}{V(\phi_0)} + \frac{M_s}{\gamma}\frac{S(\phi)-S(\phi_0)}{S(\phi_0)}f(\phi)\ , \tag{12}$$

where $g(\phi) = -\gamma^2\Delta f + (3\phi^2-1)f(\phi)$.

It is assumed in the present work that dissipation of the system energy is due to fluid viscosity, friction on the wall, and interfacial mixing due to diffuse interface representation. Accordingly, the total dissipation functional Δ is defined as follows

$$\Delta = \int_\Omega 2\eta|\boldsymbol{D}_\eta|^2 d\boldsymbol{x} + \int_\Omega \frac{1}{M_\phi}|q_\phi|^2 d\boldsymbol{x} + \int_{\partial\Omega_w}\beta_s|\mathbf{u}_{\boldsymbol{\tau}}|^2 ds + \int_{\partial\Omega_w}\kappa_\Gamma|J_\Gamma|^2 ds\ , \tag{13}$$

where the first term is the macroscopic dissipation induced by the fluid viscosity with $\boldsymbol{D}_\eta = \frac{1}{2}[\nabla\mathbf{u} + (\nabla\mathbf{u})^T]$, the second term is the microscopic dissipation induced by the diffuse interface, the third term is the boundary friction dissipation, and the last term is the dissipation induced by the diffuse interface contacting the wall.

By taking the time derivative of the total energy functional (5), it is obtained that

$$\frac{dE_{total}}{dt} = \frac{d}{dt}E_{kin} + \frac{d}{dt}E_{cell} + \frac{d}{dt}E_w \tag{14}$$

$$\equiv I_1 + I_2 + I_3\ . \tag{15}$$

This leads to

$$\begin{aligned}
I_1 &= \frac{d}{dt}\int_\Omega \frac{\rho|\mathbf{u}|^2}{2}d\boldsymbol{x} \\
&= \int_\Omega \frac{1}{2}\frac{\partial\rho}{\partial t}|\mathbf{u}|^2 d\boldsymbol{x} + \int_\Omega \rho\frac{\partial\mathbf{u}}{\partial t}\cdot\mathbf{u}d\boldsymbol{x} \\
&= \int_\Omega \frac{1}{2}\frac{\partial\rho}{\partial t}|\mathbf{u}|^2 d\boldsymbol{x} + \int_\Omega \rho\frac{d\mathbf{u}}{dt}\cdot\mathbf{u}d\boldsymbol{x} - \int_\Omega(\rho\mathbf{u}\cdot\nabla\mathbf{u})\cdot\mathbf{u}d\boldsymbol{x} \\
&= \int_\Omega \frac{1}{2}\frac{\partial\rho}{\partial t}|\mathbf{u}|^2 d\boldsymbol{x} + \int_\Omega \rho\frac{d\mathbf{u}}{dt}\cdot\mathbf{u}d\boldsymbol{x} + \int_\Omega \nabla\cdot(\rho\mathbf{u})\frac{|\mathbf{u}|^2}{2}d\boldsymbol{x} \\
&= \int_\Omega(\nabla\cdot\boldsymbol{\sigma}_\eta)\cdot\mathbf{u}d\boldsymbol{x} + \int_\Omega \mathbf{F}_\phi\cdot\mathbf{u}d\boldsymbol{x} + \int_\Omega \lambda\delta_\gamma\mathcal{P}:\nabla\mathbf{u}d\boldsymbol{x} - \int_\Omega pI:\nabla\mathbf{u}d\boldsymbol{x} \\
&= -\int_\Omega((\boldsymbol{\sigma}_\eta + pI):\nabla\mathbf{u})d\boldsymbol{x} + \int_\Omega \mathbf{F}_\phi\cdot\mathbf{u}dx - \int_\Omega\nabla\cdot(\lambda\delta_\gamma\mathcal{P})\cdot\mathbf{u}d\boldsymbol{x}
\end{aligned}$$

$$+\int_{\partial\Omega_w}((\boldsymbol{\sigma}_\eta+\lambda\delta_\gamma\mathcal{P})\cdot\mathbf{n})\cdot\mathbf{u}_\tau dS\ , \tag{16}$$

where p and λ are introduced as Lagrange multipliers accounting for fluid incompressiblity and local inextensibility of the cell membrane, respectively. δ_γ is defined in Eq. (3). The velocity boundary conditions in (4) and integration by parts are utilized in the above derivation from step 4 to step 6.

Using the first equation in Eq. set (2), and the definitions of $g(\phi)$ and $f(\phi)$ give rise to

$$\begin{aligned}
I_2 &= \frac{d}{dt}\int_\Omega \frac{\hat\kappa_B}{2\gamma}\left|\frac{f(\phi)}{\gamma}\right|^2 d\boldsymbol{x}+\frac{d}{dt}\left(\frac{M_v}{2}\frac{(V(\phi)-V(\phi_0))^2}{V(\phi_0)}+\frac{M_s}{2}\frac{(S(\phi)-S(\phi_0))^2}{S(\phi_0)}\right)\\
&= \int_\Omega \frac{\hat\kappa_B}{\gamma}\frac{f}{\gamma^2}\frac{\partial f}{\partial t}d\boldsymbol{x}+M_v\int_\Omega\frac{V(\phi)-V(\phi_0)}{V(\phi_0)}\frac{\partial\phi}{\partial t}d\boldsymbol{x}+M_s\int_\Omega\frac{S(\phi)-S(\phi_0)}{S(\phi_0)}\frac{\partial S(\phi)}{\partial t}d\boldsymbol{x}\\
&= \int_\Omega \frac{\hat\kappa_B}{\gamma}\frac{f}{\gamma^2}\left(-\gamma^2\Delta\left(\frac{\partial\phi}{\partial t}\right)+(3\phi^2-1)\frac{\partial\phi}{\partial t}\right)d\boldsymbol{x}\\
&\quad +M_v\int_\Omega\frac{V(\phi)-V(\phi_0)}{V(\phi_0)}\frac{\partial\phi}{\partial t}d\boldsymbol{x}\\
&\quad +M_s\int_\Omega\frac{S(\phi)-S(\phi_0)}{S(\phi_0)}\frac{1}{\gamma}\left(\gamma^2\nabla\phi\cdot\nabla\frac{\partial\phi}{\partial t}+(\phi^2-1)\phi\frac{\partial\phi}{\partial t}\right)d\boldsymbol{x}\\
&= \int_\Omega \frac{\hat\kappa_B}{\gamma^3}\left(-\gamma^2\Delta f+(3\phi^2-1)f\right)\frac{\partial\phi}{\partial t}d\boldsymbol{x}\\
&\quad +M_v\int_\Omega\frac{V(\phi)-V(\phi_0)}{V(\phi_0)}\frac{\partial\phi}{\partial t}d\boldsymbol{x}\\
&\quad +M_s\int_\Omega\frac{S(\phi)-S(\phi_0)}{S(\phi_0)}\frac{1}{\gamma}\left(-\gamma^2\Delta\phi+(\phi^2-1)\phi\right)\frac{\partial\phi}{\partial t}d\boldsymbol{x}\\
&\quad -\int_{\partial\Omega_w}\frac{\hat\kappa_B}{\gamma}f\frac{\partial}{\partial t}(\partial_n\phi)ds+\int_{\partial\Omega_w}\frac{\hat\kappa_B}{\gamma}\partial_n f\frac{\partial\phi}{\partial t}ds+M_s\int_{\partial\Omega_w}\frac{S(\phi)-S(\phi_0)}{S(\phi_0)}\gamma\partial_n\phi\frac{\partial\phi}{\partial t}ds\\
&= \int_\Omega\mu\frac{\partial\phi}{\partial t}d\boldsymbol{x}-\int_{\partial\Omega_w}\frac{\hat\kappa_B}{\gamma}f\frac{\partial}{\partial t}(\partial_n\phi)ds\\
&\quad +\int_{\partial\Omega_w}\frac{\hat\kappa_B}{\gamma}\partial_n f\frac{\partial\phi}{\partial t}ds+M_s\int_{\partial\Omega_w}\frac{S(\phi)-S(\phi_0)}{S(\phi_0)}\gamma\partial_n\phi\frac{\partial\phi}{\partial t}ds\\
&= \int_\Omega\mu q_\phi d\boldsymbol{x}-\int_\Omega\mu\mathbf{u}\cdot\nabla\phi d\boldsymbol{x}\\
&\quad +\int_{\partial\Omega_w}\frac{\hat\kappa_B}{\gamma}\partial_n f\frac{\partial\phi}{\partial t}ds+M_s\int_{\partial\Omega_w}\frac{S(\phi)-S(\phi_0)}{S(\phi_0)}\gamma\partial_n\phi\frac{\partial\phi}{\partial t}ds\ .
\end{aligned}\tag{17}$$

Here the second and third equations in the boundary conditions (4) and integration by parts are used in step 4 in the above derivation.

For I_3 in Eq. (14), it is easy to see that

$$I_3=\int_{\partial\Omega_w}\frac{\partial f_w}{\partial\phi}\frac{\partial\phi}{\partial t}ds\ . \tag{18}$$

Combining Eqs. (16) to (18) yields

$$\frac{d}{dt}E_{total} = -\int_\Omega((\boldsymbol{\sigma}_\eta+pI):\nabla\mathbf{u})d\boldsymbol{x}+\int_\Omega(\mathbf{F}_\phi-\mu\nabla\phi-\nabla\cdot(\lambda\delta_\gamma\mathcal{P}))\cdot\mathbf{u}d\boldsymbol{x}+\int_\Omega\mu q_\phi d\boldsymbol{x}$$

$$
\begin{aligned}
&+\int_{\partial\Omega_w}((\boldsymbol{\sigma}_\eta+\lambda\delta_\gamma\mathcal{P})\cdot\mathbf{n})\cdot\mathbf{u}_\tau ds+\int_{\partial\Omega_s}\hat{L}(\phi)\frac{\partial\phi}{\partial t}ds\\
=\;&-\int_\Omega((\boldsymbol{\sigma}_\eta+pI):\nabla\mathbf{u})d\boldsymbol{x}+\int_\Omega(\mathbf{F}_\phi-\mu\nabla\phi-\nabla\cdot(\lambda\delta_\gamma\mathcal{P}))\cdot\mathbf{u}d\boldsymbol{x}+\int_\Omega\mu q_\phi d\boldsymbol{x}\\
&+\int_{\partial\Omega_w}((\boldsymbol{\sigma}_\eta+\lambda\delta_\gamma\mathcal{P})\cdot\mathbf{n})\cdot\mathbf{u}_\tau ds+\int_{\partial\Omega_s}\hat{L}(\phi)(-\mathbf{u}\cdot\nabla_\Gamma\phi+J_\Gamma)ds\\
=\;&-\int_\Omega((\boldsymbol{\sigma}_\eta+pI):\nabla\mathbf{u})d\boldsymbol{x}+\int_\Omega(\mathbf{F}_\phi-\mu\nabla\phi-\nabla\cdot(\lambda\delta_\gamma\mathcal{P}))\cdot\mathbf{u}d\boldsymbol{x}+\int_\Omega\mu q_\phi d\boldsymbol{x}\\
&+\int_{\partial\Omega_w}((\boldsymbol{\sigma}_\eta+\lambda\delta_\gamma\mathcal{P})\cdot\mathbf{n}-\hat{L}(\phi)\nabla_\Gamma\phi)\cdot\mathbf{u}_\tau ds+\int_{\partial\Omega_w}\hat{L}(\phi)J_\Gamma ds\ ,
\end{aligned}
\tag{19}
$$

where $\hat{L}(\phi)=\dfrac{\hat{\kappa}_B}{\gamma}\partial_n f+M_s\dfrac{S(\phi)-S(\phi_0)}{S(\phi_0)}\gamma\partial_n\phi+\dfrac{\partial f_w}{\partial\phi}$.

Using the energy dissipation law $\frac{dE_{total}}{dt}=-\Delta$ [72, 20], and the definition of the dissipation functional (13), it is obtained that

$$
\begin{cases}
\boldsymbol{\sigma}_\eta=2\eta\boldsymbol{D}_\eta-pI\ , & \text{in }\Omega\ ,\\
q_\phi=-M_\phi\mu\ , & \text{in }\Omega\ ,\\
\mathbf{F}_\phi=\mu\nabla\phi+\nabla\cdot(\lambda\delta_\gamma\mathcal{P})\ , & \text{in }\Omega\ ,\\
J_\Gamma=-\kappa_\Gamma^{-1}\hat{L}(\phi)\ , & \text{on }\partial\Omega_w\ ,\\
u_{\tau_i}=\beta_s^{-1}(-(\mathbf{n}\cdot(\boldsymbol{\sigma}_\eta+\lambda\delta_\gamma\mathcal{P})\cdot\boldsymbol{\tau}_i)+\hat{L}(\phi)\partial_{\tau_i}\phi)\ ,\ i=1,2, & \text{on }\partial\Omega_w\ .
\end{cases}
\tag{20}
$$

Here constant M_ϕ is called the mobility (a phenomenological parameter), κ_γ is the boundary mobility (a phenomenological parameter) and β_s is the wall friction coefficient.

To this end, the proposed phase-field model is composed of the following equations

$$
\begin{cases}
\frac{\partial\phi}{\partial t}+\nabla\cdot(\mathbf{u}\phi)=-M_\phi\mu\ ,\\
\mu=\frac{\hat{\kappa}_B}{\gamma^3}g(\phi)+M_v\frac{V(\phi)-V(\phi_0)}{V(\phi_0)}+\frac{M_s}{\gamma}\frac{S(\phi)-S(\phi_0)}{S(\phi_0)}f(\phi)\ ,\\
g(\phi)=-\gamma^2\Delta f+(3\phi^2-1)f(\phi),\\
f(\phi)=-\gamma^2\Delta\phi+(\phi^2-1)\phi\ ,\\
\rho(\frac{\partial\mathbf{u}}{\partial t}+(\mathbf{u}\cdot\nabla)\mathbf{u})+\nabla p=\nabla\cdot(2\eta\boldsymbol{D}_\eta)+\mu\nabla\phi+\nabla\cdot(\lambda\delta_\gamma\mathcal{P})\ ,\\
\nabla\cdot\mathbf{u}=0\ ,\\
\delta_\gamma(\mathcal{P}:\nabla\mathbf{u})=0\ ,
\end{cases}
\tag{21}
$$

with the boundary conditions

$$
\begin{cases}
\mathbf{u}\cdot\mathbf{n}=0\ ,\\
-\beta_s u_{\tau_i}=(\mathbf{n}\cdot(\boldsymbol{\sigma}_\eta+\lambda\delta_\gamma\mathcal{P})\cdot\boldsymbol{\tau}_i)-\hat{L}(\phi)\partial_{\tau_i}\phi\ ,\ i=1,2,\\
f=0\ ,\\
\kappa_\Gamma\left(\frac{\partial\phi}{\partial t}+\mathbf{u}\cdot\nabla_\Gamma\phi\right)=-\hat{L}(\phi)\ ,\\
\hat{L}(\phi)=\frac{\hat{\kappa}_B}{\gamma}\partial_n f+M_s\frac{S(\phi)-S(\phi_0)}{S(\phi_0)}\gamma\partial_n\phi+\frac{\partial f_w}{\partial\phi}\ ,\\
\partial_n\lambda=0\ .
\end{cases}
\tag{22}
$$

3 Dimentionless Model Governing Equations and Energy Dissipation Law

If the viscosity, length, velocity, time, bulk and boundary chemical potentials in Eqs. (21)-(22) are scaled by their corresponding characteristic values η_0, L, U, $\frac{L}{U}$ $\frac{\eta_0 U}{L}$ and $\eta_0 U$, respectively, Eqs. (21)-(22) can be rewritten as

$$\begin{cases} Re(\frac{\partial \mathbf{u}}{\partial t} + (\mathbf{u}\cdot\nabla)\mathbf{u}) + \nabla P = \nabla\cdot(2\eta \boldsymbol{D}) + \mu\nabla\phi + \nabla\cdot(\lambda\delta_\epsilon \mathcal{P}) \ , & \text{in } \Omega \ , \\ \nabla\cdot\mathbf{u} = 0 \ , & \text{in } \Omega \ , \\ \frac{\partial\phi}{\partial t} + \mathbf{u}\cdot\nabla\phi = -\mathcal{M}\mu \ , & \text{in } \Omega \ , \\ \mu = \kappa_B g(\phi) + \mathcal{M}_v \frac{(V(\phi)-V(\phi_0))}{V(\phi_0)} + \mathcal{M}_s \frac{(S(\phi)-S(\phi_0))}{S(\phi_0)} f(\phi) \ , & \text{in } \Omega \ , \\ f(\phi) = -\epsilon\Delta\phi + \frac{(\phi^2-1)}{\epsilon}\phi, \ g(\phi) = -\Delta f + \frac{1}{\epsilon^2}(3\phi^2-1)f(\phi) \ , & \text{in } \Omega \ , \\ \delta_\epsilon(\mathcal{P}:\nabla\mathbf{u}) = 0 \ , & \text{in } \Omega \ , \end{cases} \tag{23}$$

with the boundary conditions

$$\begin{cases} \kappa\dot{\phi} + L(\phi) = 0 \ , & \text{on } \partial\Omega_w \ , \\ L(\phi) = \kappa_B\partial_n f + \epsilon\mathcal{M}_s\frac{S(\phi)-S(\phi_0)}{S(\phi_0)}\partial_n\phi + \alpha_w\frac{df_w}{d\phi} \ , & \text{on } \partial\Omega_w \ , \\ -l_s^{-1}u_{\tau_i} = \boldsymbol{\tau_i}\cdot(2\eta\mathbf{D}_\eta + \lambda\delta_\epsilon\mathcal{P})\cdot\boldsymbol{n} - L(\phi)\partial_{\tau_i}\phi \ , \ i=1,2, & \text{on } \partial\Omega_w \ , \\ f = 0 \ , & \text{on } \partial\Omega_w \ , \\ \partial_n\lambda = 0 \ , & \text{on } \partial\Omega_w \ , \end{cases} \tag{24}$$

where $V(\phi) = \int_\Omega \phi d\boldsymbol{x}$, $S(\phi) = \int_\Omega \frac{\epsilon}{2}|\nabla\phi|^2 + \frac{1}{4\epsilon}(\phi^2-1)^2 d\boldsymbol{x}$ and $\delta_\epsilon = \frac{1}{2}\epsilon^2|\nabla\phi|^2$. The dimensionless constants appeared in Eqs. (23)-(24) are given by $\epsilon = \frac{\gamma}{L}$, $Re = \frac{\rho_0 UL}{\eta_0}$, $\mathcal{M} = M_\phi\eta_0$, $\kappa_B = \frac{\hat{\kappa}_B}{L^2\eta_0 U}$, $k = \frac{\hat{\kappa}_B}{\eta_0 L}$, $l_s = \frac{\eta_0}{\beta_s L}$, $\alpha_w = \frac{\sigma}{\eta_0 U}$, $\mathcal{M}_s = \frac{M_s}{\eta_0 U}$, and $\mathcal{M}_v = \frac{M_v L}{\eta_0 U}$.

If we define the Sobolev spaces as follows

$$\boldsymbol{W}^{1,3} = (W^{1,3})^2, \tag{25}$$

$$\boldsymbol{W}^{1,3}(\Omega) = \left\{\mathbf{u} = (u_x, u_y)^T \in \boldsymbol{W}^{1,3} | \mathbf{u}\cdot\boldsymbol{n} = 0, \text{ on } \partial\Omega_w\right\}, \tag{26}$$

$$\boldsymbol{W}_b = W^{1,3}(\Omega)\times W^{1,3}(\Omega)\times W^{1,3}(\Omega)\times W^{1,3/2}(\Omega)\times W^{1,3/2}(\Omega)\times \boldsymbol{W}^{1,3}(\Omega), \tag{27}$$

and norms $\|f\| = \left(\int_\Omega |f|^2 d\boldsymbol{x}\right)^{\frac{1}{2}}$ and $\|f\|_w = \left(\int_{\partial\Omega_w} |f|^2 ds\right)^{\frac{1}{2}}$ be the L^2 norm defined in the domain and on the domain boundary respectively, then the system (23)-(24) satisfies the following energy law.

Theorem 3.1. *If* $(\phi,\ f,\ \mu,\ \lambda,\ P,\ \mathbf{u}) \in \boldsymbol{W}_b$ *are smooth solutions of the above system* (23)-(24)*, then the following energy law is satisfied:*

$$\frac{d}{dt}\mathcal{E}_{total} \ = \ \frac{d}{dt}(\mathcal{E}_{kin} + \mathcal{E}_{cell} + \mathcal{E}_w)$$

$$= -2\|\eta^{1/2}\mathbf{D}_\eta\|^2 - \mathcal{M}\|\mu\|^2 - \kappa\|\dot{\phi}\|_w^2 - \|l_s^{-1/2}\mathbf{u}_\tau\|_w^2 \ , \tag{28}$$

where $\mathcal{E}_{total} = \mathcal{E}_{kin} + \mathcal{E}_{cell} + \mathcal{E}_w$, $\mathcal{E}_{kin} = \frac{1}{2}\int_\Omega |\mathbf{u}|^2 d\boldsymbol{x}$, $\mathcal{E}_{cell} = \frac{\kappa_B}{2\epsilon}\int_\Omega |f|^2 d\boldsymbol{x} + \mathcal{M}_v \frac{(V(\phi)-V(\phi_0))^2}{2V(\phi_0)} + \mathcal{M}_s \frac{(S(\phi)-S(\phi_0))^2}{2S(\phi_0)}$ *and* $\mathcal{E}_w = \alpha_w \int_{\partial\Omega_w} f_w ds$.

Proof: Multiplying the first equation in Eq. (23) with $\mathbf{u}$ and integration by parts yield

$$\begin{aligned}
\frac{d}{dt}\mathcal{E}_{kin} &= -\int_\Omega 2\eta|\boldsymbol{D}_\eta|^2 d\boldsymbol{x} + \int_{\partial\Omega_w} (\boldsymbol{\sigma}_\eta \cdot \mathbf{n})\cdot \mathbf{u}_\tau ds + \int_\Omega \mu\nabla\phi\cdot\mathbf{u} d\boldsymbol{x} - \int_\Omega \lambda\delta_\epsilon\mathcal{P} : \nabla\mathbf{u} d\boldsymbol{x} \\
&\quad + \int_{\partial\Omega_w} (\lambda\delta_\epsilon\mathcal{P}\cdot\mathbf{n})\cdot\mathbf{u}_\tau ds \\
&= -\int_\Omega 2\eta|\boldsymbol{D}_\eta|^2 d\boldsymbol{x} - \int_\Omega \lambda\delta_\epsilon\mathcal{P} : \nabla\mathbf{u} d\boldsymbol{x} - l_s^{-1}\int_{\partial\Omega_w} |\mathbf{u}_\tau|^2 ds \\
&\quad + \int_{\partial\Omega_w} L(\phi)\partial_\tau\phi\cdot\mathbf{u}_\tau ds + \int_\Omega \mu\nabla\phi\cdot\mathbf{u} d\boldsymbol{x} \ ,
\end{aligned} \tag{29}$$

where the slip boundary condition in Eq. (24) is applied.

Taking the inner product of the third equation in Eq. (23) with μ results in

$$\int_\Omega \frac{\partial\phi}{\partial t}\mu d\boldsymbol{x} + \int_\Omega \mathbf{u}\cdot\nabla\phi\mu d\boldsymbol{x} = -\mathcal{M}\int_\Omega |\mu|^2 d\boldsymbol{x} \ . \tag{30}$$

Multiplying the fourth equation in Eq. (23) with $\frac{\partial\phi}{\partial t}$ and integration by part give rise to

$$\begin{aligned}
\int_\Omega \mu\frac{\partial\phi}{\partial t} d\boldsymbol{x} &= \kappa_B\int_\Omega g\frac{\partial\phi}{\partial t} d\boldsymbol{x} + \frac{d}{dt}\left(\mathcal{M}_v\frac{(V(\phi)-V(\phi_0))^2}{2V(\phi_0)}\right) + \mathcal{M}_s\frac{S(\phi)-S(\phi_0)}{S(\phi_0)}\int_\Omega f\frac{\partial\phi}{\partial t} d\boldsymbol{x} \\
&= \kappa_B\int_\Omega f\frac{\partial}{\partial t}\left(-\Delta\phi + \frac{1}{\epsilon^2}(\phi^3-\phi)\right) d\boldsymbol{x} - \kappa_B\int_{\partial\Omega_w}\partial_n f\frac{\partial\phi}{\partial t} ds \\
&\quad + \frac{d}{dt}\left(\mathcal{M}_v\frac{(V(\phi)-V(\phi_0))^2}{V(\phi_0)}\right) + \mathcal{M}_s\frac{d}{dt}\left(\frac{(S(\phi)-S(\phi_0))^2}{2S(\phi_0)}\right) \\
&\quad - \mathcal{M}_s\left(\frac{S(\phi)-S(\phi_0)}{S(\phi_0)}\right)\int_{\partial\Omega_w}\epsilon\partial_n\phi\frac{\partial\phi}{\partial t} ds \\
&= \frac{d}{dt}\left(\kappa_B\int_\Omega \frac{|f|^2}{2\epsilon} d\boldsymbol{x}\right) + \frac{d}{dt}\left(\mathcal{M}_v\frac{(V(\phi)-V(\phi_0))^2}{2V(\phi_0)}\right) \\
&\quad + \mathcal{M}_s\frac{d}{dt}\left(\frac{(S(\phi)-S(\phi_0))^2}{2S(\phi_0)}\right) - \int_{\partial\Omega_w} L(\phi)\frac{\partial\phi}{\partial t} ds + \alpha_w\frac{d}{dt}\int_{\partial\Omega_w} f_w ds \\
&= \frac{d}{dt}(\mathcal{E}_{cell}+\mathcal{E}_w) - \int_{\partial\Omega_w} L(\phi)\frac{\partial\phi}{\partial t} ds \ ,
\end{aligned} \tag{31}$$

where the definitions of $f(\phi)$, $g(\phi)$ and the boundary conditions of ϕ and f are utilized.

Multiplying the last equations with λ and integration by parts leads to

$$\int_\Omega (\lambda\delta_\epsilon\mathcal{P}) : \nabla\mathbf{u} d\boldsymbol{x} = 0 \ . \tag{32}$$

Finally, the energy dissipation law (28) is obtained by combining Eqs. (29), (30), (31) and (32). ■

4 Numerical Scheme and Discrete Energy law

4.1 Time-discrete primitive method

The numerical scheme for solving Eqs. (23)-(24) uses the mid-point method for temporal discretization. Let Δt denote the time step size, $()^{n+1}$ and $()^n$ denote the value of the variables at times $(n+1)\Delta t$ and $n\Delta t$, respectively. The semi-discrete in time equations are as follows:

$$\begin{cases} \frac{\mathbf{u}^{n+1}-\mathbf{u}^n}{\Delta t} + (\mathbf{u}^{n+\frac{1}{2}}\cdot\nabla)\mathbf{u}^{n+\frac{1}{2}} + \frac{1}{Re}\nabla P^{n+\frac{1}{2}} = \frac{1}{Re}\nabla\cdot(\eta^n(\nabla\mathbf{u}^{n+\frac{1}{2}} + (\nabla\mathbf{u}^{n+\frac{1}{2}})^T)) \\ +\frac{1}{Re}\mu^{n+\frac{1}{2}}\nabla\phi^{n+\frac{1}{2}} + \frac{1}{Re}\nabla\cdot\left(\lambda^{n+\frac{1}{2}}\mathcal{P}^n\delta_\epsilon\right) , & \text{in } \Omega , \\ \nabla\cdot\mathbf{u}^{n+\frac{1}{2}} = 0 , & \text{in } \Omega , \\ \frac{\phi^{n+1}-\phi^n}{\Delta t} + (\mathbf{u}^{n+\frac{1}{2}}\cdot\nabla)\phi^{n+\frac{1}{2}} = -\mathcal{M}\mu^{n+\frac{1}{2}} , & \text{in } \Omega , \\ \mu^{n+\frac{1}{2}} = \kappa_B g(\phi^{n+1},\phi^n) + \mathcal{M}_v\frac{(V(\phi^{n+\frac{1}{2}})-V(\phi_0))}{V(\phi_0)} + \mathcal{M}_s\frac{(S(\phi^{n+\frac{1}{2}})-S(\phi_0))}{S(\phi_0)}f(\phi^{n+1},\phi^n) , & \text{in } \Omega , \\ f^{n+\frac{1}{2}} = -\epsilon\Delta\phi^{n+\frac{1}{2}} + \frac{1}{\epsilon}((\phi^{n+\frac{1}{2}})^2-1)\phi^{n+\frac{1}{2}} , & \text{in } \Omega , \\ \xi\epsilon^2\nabla\cdot((\phi^n)^2\nabla\lambda^{n+\frac{1}{2}}) + \delta_\epsilon\mathcal{P}^n : \nabla\mathbf{u}^{n+\frac{1}{2}} = 0 , & \text{in } \Omega . \end{cases} \tag{33}$$

The numerical boundary conditions can be written as:

$$\begin{cases} \kappa\dot{\phi}^{n+\frac{1}{2}} = -L^{n+\frac{1}{2}} , & \text{on } \partial\Omega_w , \\ L^{n+\frac{1}{2}} = \kappa_B\partial_n f^{n+\frac{1}{2}} + \mathcal{M}_s\epsilon\frac{S(\phi^{n+\frac{1}{2}})-S_0}{S_0}\partial_n\phi^{n+\frac{1}{2}} + \alpha_w\frac{f_w^{n+1}-f_w^n}{\phi^{n+1}-\phi^n} , & \text{on } \partial\Omega_w , \\ -l_s^{-1}u_{\tau_i}^{n+\frac{1}{2}} = \boldsymbol{\tau_i}\cdot(\eta^n(\nabla\mathbf{u}^{n+\frac{1}{2}} + (\nabla\mathbf{u}^{n+\frac{1}{2}})^T) + \lambda^{n+\frac{1}{2}}\delta_\epsilon\mathcal{P}^n)\cdot\boldsymbol{n} \\ \qquad\qquad - L^{n+\frac{1}{2}}\partial_{\tau_i}\phi^{n+\frac{1}{2}} , \quad i=1,2, & \text{on } \partial\Omega_w , \\ f^{n+\frac{1}{2}} = 0 , & \text{on } \partial\Omega_w , \\ \partial_n\lambda^{n+\frac{1}{2}} = 0 , & \text{on } \partial\Omega_w , \end{cases} \tag{34}$$

where

$$f(\phi^{n+1},\phi^n) = -\epsilon\Delta\phi^{n+\frac{1}{2}} + \frac{1}{4\epsilon}((\phi^{n+1})^2 + (\phi^n)^2 - 2)(\phi^{n+1}+\phi^n) , \tag{35}$$

$$g(\phi^{n+1},\phi^n) = \left(-\Delta f^{n+\frac{1}{2}} + \frac{1}{\epsilon^2}\left((\phi^{n+1})^2 + (\phi^n)^2 + \phi^{n+1}\phi^n - 1\right)f^{n+\frac{1}{2}}\right) , \tag{36}$$

$(\cdot)^{n+\frac{1}{2}} = \frac{(\cdot)^n+(\cdot)^{n+1}}{2}$ and $\mathcal{P}^n = I - \mathbf{n}_m^n\otimes\mathbf{n}_m^n$ with $\mathbf{n}_m^n = \frac{\nabla\phi^n}{|\nabla\phi^n|}$.

Remark 4.1. *Here an extra term $\xi\epsilon^2\nabla\cdot((\phi^n)^2\nabla\lambda^{n+\frac{1}{2}})$ is introduced to extend λ to the whole domain as in [1]. This can be regarded as a relaxation for the local inextensibility near the membrane. The last equation can also be derived directly by the variational method described in Section 2 by adding an extra dissipation term $\int_\Omega\xi\epsilon^2|\phi\nabla\lambda|^2 d\boldsymbol{x}$ in the dissipation functional.*

The above scheme obeys the following theorem of energy stability.

Theorem 4.1. *If $(\phi^n, \mathbf{u}^n, P^n)$ are smooth solutions of the above system (33)-(34), then the following energy law is satisfied:*

$$\begin{aligned}\mathcal{E}_{total}^{n+1} - \mathcal{E}_{total}^{n} &= (\mathcal{E}_{kin}^{n+1} + \mathcal{E}_{cell}^{n+1} + \mathcal{E}_{w}^{n+1}) - (\mathcal{E}_{kin}^{n} + \mathcal{E}_{cell}^{n} + \mathcal{E}_{w}^{n}) \\ &= \frac{\triangle t}{Re}\Big(-2\|(\eta^n)^{1/2}\mathbf{D}_\eta^{n+\frac{1}{2}}\|^2 - \mathcal{M}\|\mu^{n+\frac{1}{2}}\|^2 - \xi\| \ \epsilon\phi^n\nabla\lambda^{n+\frac{1}{2}}\|^2 \\ &\quad -\frac{1}{\kappa}\|L(\phi^{n+\frac{1}{2}})\|_w^2 - \|l_s^{-1/2}\mathbf{u}_\tau^{n+\frac{1}{2}}\|_w^2\Big) \ , \end{aligned} \tag{37}$$

where $\mathcal{E}_{total}^n = \mathcal{E}_{kin}^n + \mathcal{E}_{cell}^n + \mathcal{E}_w^n$ *with* $\mathcal{E}_{kin}^n = \frac{1}{2}\|\mathbf{u}^n\|^2$, $\mathcal{E}_{cell}^n = \frac{\kappa_B\|f^n\|^2}{2\epsilon} + \mathcal{M}_v\frac{(V(\phi^n)-V(\phi_0))^2}{2V(\phi_0)} + \mathcal{M}_s\frac{(S(\phi^n)-S(\phi_0))^2}{2S(\phi_0)}$ *and* $\mathcal{E}_w^n = \alpha_w\int_{\partial\Omega_w} f_w^n ds$.

The following two lemmas are needed for proving **Theorem 4.1**.

Lemma 4.2. *Let*

$$f(\phi^{n+1},\phi^n) = -\epsilon\Delta\phi^{n+\frac{1}{2}} + \frac{1}{4\epsilon}((\phi^{n+1})^2 + (\phi^n)^2 - 2)(\phi^{n+1} + \phi^n) \ . \tag{38}$$

Then $f(\phi^{n+1},\phi^n)$ satisfies

$$\int_\Omega f(\phi^{n+1},\phi^n)(\phi^{n+1}-\phi^n)d\boldsymbol{x} = S^{n+1} - S^n - \int_{\partial\Omega_w}\epsilon\partial_n\phi^{n+\frac{1}{2}}(\phi^{n+1}-\phi^n)ds \ , \tag{39}$$

where $S^{n+1} = \int_\Omega G(\phi^{n+1})d\boldsymbol{x}, S^n = \int_\Omega G(\phi^n)d\boldsymbol{x}$.

Proof:

$$\begin{aligned} &\int_\Omega f(\phi^{n+1},\phi^n)(\phi^{n+1}-\phi^n)d\boldsymbol{x} \\ =& \int_\Omega\left(\epsilon\Delta\phi^{n+\frac{1}{2}}(\phi^{n+1}-\phi^n) + \frac{1}{4\epsilon}((\phi^{n+1})^2 + (\phi^n)^2 - 2)(\phi^{n+1}+\phi^n)(\phi^{n+1}-\phi^n)\right)d\boldsymbol{x} \\ =& \int_\Omega \epsilon\nabla\phi^{n+\frac{1}{2}}\cdot\nabla(\phi^{n+1}-\phi^n)d\boldsymbol{x} - \int_{\partial\Omega_W}\epsilon\partial_n\phi^{n+\frac{1}{2}}(\phi^{n+1}-\phi^n)ds \\ &+\int_\Omega\frac{1}{4\epsilon}((\phi^{n+1})^4 - 2(\phi^{n+1})^2 - (\phi^n)^4 + 2(\phi^n)^2)d\boldsymbol{x} \\ =& \int_\Omega\left[\frac{\epsilon}{2}((\nabla\phi^{n+1})^2 - (\nabla\phi^n)^2) + \frac{1}{4\epsilon}(((\phi^{n+1})^2-1)^2 - ((\phi^n)^2-1)^2)\right]d\boldsymbol{x} \\ &-\int_{\partial\Omega_W}\epsilon\partial_n\phi^{n+\frac{1}{2}}(\phi^{n+1}-\phi^n)ds \\ =& \int_\Omega\left(\frac{\epsilon}{2}(\nabla\phi^{n+1})^2 + \frac{1}{4\epsilon}(\phi^{n+1}-1)^2\right)d\boldsymbol{x} - \int_\Omega\left(\frac{\epsilon}{2}(\nabla\phi^n)^2 + \frac{1}{4\epsilon}(\phi^n-1)^2\right)d\boldsymbol{x} \\ &-\int_{\partial\Omega_w}\epsilon\partial_n\phi^{n+\frac{1}{2}}(\phi^{n+1}-\phi^n)ds \\ =& \ S^{n+1} - S^n - \int_{\partial\Omega_w}\epsilon\partial_n\phi^{n+\frac{1}{2}}(\phi^{n+1}-\phi^n)ds \ . \end{aligned}$$

■

Lemma 4.3. *Let*

$$g(\phi^{n+1},\phi^n) = -\Delta f^{n+\frac{1}{2}} + \frac{1}{\epsilon^2}((\phi^{n+1})^2 + (\phi^n)^2 + \phi^{n+1}\phi^n - 1)f^{n+\frac{1}{2}} \ . \tag{40}$$

Then $g(\phi^{n+1},\phi^n)$ *satisfies*

$$\int_\Omega g(\phi^{n+1},\phi^n)(\phi^{n+1}-\phi^n)d\boldsymbol{x} = \int_\Omega \frac{1}{2\epsilon}((f^{n+1})^2 - (f^n)^2)d\boldsymbol{x} - \int_{\partial\Omega_w} \partial_n f^{n+\frac{1}{2}}(\phi^{n+1}-\phi^n)ds \ , \tag{41}$$

where $f^{n+1} = -\epsilon\Delta\phi^{n+1} + \frac{1}{\epsilon}((\phi^{n+1})^2-1)\phi^{n+1}$, $f^n = -\epsilon\Delta\phi^n + \frac{1}{\epsilon}((\phi^n)^2-1)\phi^n$.
Proof:

$$\begin{aligned}
&\int_\Omega g(\phi^{n+1},\phi^n)(\phi^{n+1}-\phi^n)d\boldsymbol{x}\\
=\ &\int_\Omega \nabla f^{n+\frac{1}{2}}\nabla(\phi^{n+1}-\phi^n)d\boldsymbol{x} - \int_{\partial\Omega_w}\partial_n f^{n+\frac{1}{2}}(\phi^{n+1}-\phi^n)ds\\
&+\int_\Omega \frac{1}{\epsilon^2} f^{n+\frac{1}{2}}(((\phi^{n+1})^2-1)\phi^{n+1} - ((\phi^n)^2-1)\phi^n)d\boldsymbol{x}\\
=\ &-\int_\Omega f^{n+\frac{1}{2}}\Delta(\phi^{n+1}-\phi^n)d\boldsymbol{x} - \int_{\partial\Omega_w}\partial_n f^{n+\frac{1}{2}}(\phi^{n+1}-\phi^n)ds\\
&+\int_\Omega \frac{1}{\epsilon^2} f^{n+\frac{1}{2}}(((\phi^{n+1})^2-1)\phi^{n+1} - ((\phi^n)^2-1)\phi^n)d\boldsymbol{x}\\
=\ &\int_\Omega \frac{1}{\epsilon} f^{n+\frac{1}{2}}\left((-\epsilon\Delta\phi^{n+1} + \frac{1}{\epsilon}((\phi^{n+1})^2-1)\phi^{n+1}) - (-\epsilon\Delta\phi^n + \frac{1}{\epsilon}((\phi^n)^2-1)\phi^n)\right)d\boldsymbol{x}\\
&-\int_{\partial\Omega_w}\partial_n f^{n+\frac{1}{2}}(\phi^{n+1}-\phi^n)ds\\
=\ &\int_\Omega \frac{1}{2\epsilon}(f^{n+1}+f^n)(f^{n+1}-f^n)d\boldsymbol{x} - \int_{\partial\Omega_w}\partial_n f^{n+\frac{1}{2}}(\phi^{n+1}-\phi^n)ds\\
=\ &\int_\Omega \frac{1}{2\epsilon}((f^{n+1})^2-(f^n)^2)d\boldsymbol{x} - \int_{\partial\Omega_w}\partial_n f^{n+\frac{1}{2}}(\phi^{n+1}-\phi^n)ds \ .
\end{aligned}$$

■

Proof of Theorem 4.1: Multiplying the first equation in system (33) by $\Delta t\mathbf{u}^{n+\frac{1}{2}}$ gives

$$\begin{aligned}
&\int_\Omega \frac{1}{2}((\mathbf{u}^{n+1})^2 - (\mathbf{u}^n)^2)d\boldsymbol{x} + \int_\Omega \Delta t\mathbf{u}^{n+\frac{1}{2}}\cdot((\mathbf{u}^{n+\frac{1}{2}}\nabla)\cdot\mathbf{u}^{n+\frac{1}{2}})d\boldsymbol{x} - \frac{\Delta t}{Re}\int_\Omega P^{n+\frac{1}{2}}\nabla\cdot\mathbf{u}^{n+\frac{1}{2}}d\boldsymbol{x}\\
=\ &-\frac{\Delta t}{Re}\int_\Omega \nabla\mathbf{u}^{n+\frac{1}{2}} : \eta^n(\nabla\mathbf{u}^{n+\frac{1}{2}} + (\nabla\mathbf{u}^{n+\frac{1}{2}})^T)d\boldsymbol{x} + \frac{\Delta t}{Re}\int_\Omega \mathbf{u}^{n+\frac{1}{2}}\cdot\nabla\phi^{n+\frac{1}{2}}\mu^{n+\frac{1}{2}}d\boldsymbol{x}\\
&-\frac{\Delta t}{Re}\int_\Omega \lambda^{n+\frac{1}{2}}\delta_\epsilon\mathcal{P}^n : \nabla\mathbf{u}^{n+\frac{1}{2}}d\boldsymbol{x} + \frac{\Delta t}{Re}\int_{\partial\Omega_w}\lambda^{n+\frac{1}{2}}(\delta_\epsilon\mathcal{P}^n\cdot\mathbf{n})\cdot\mathbf{u}_\tau^{n+\frac{1}{2}}ds\\
&+\frac{\Delta t}{Re}\int_{\partial\Omega_w}\mathbf{u}^{n+\frac{1}{2}}\cdot\eta^n((\nabla\mathbf{u}^{n+\frac{1}{2}} + (\nabla\mathbf{u}^{n+\frac{1}{2}})^T)\cdot\boldsymbol{n})ds \ .
\end{aligned} \tag{42}$$

Multiplying the fourth equation in system (33) by $\frac{\phi^{n+1}-\phi^n}{Re}$ and integration by parts lead to

$$\frac{1}{Re}\int_\Omega \mu^{n+\frac{1}{2}}(\phi^{n+1}-\phi^n)d\boldsymbol{x} = \frac{\kappa_B}{Re}\int_\Omega \frac{1}{2\epsilon}((f^{n+1})^2-(f^n)^2)d\boldsymbol{x}$$
$$+\frac{\mathcal{M}_v}{Re}\frac{(V(\phi^{n+1})-V_0)^2-(V(\phi^n)-V_0)^2}{2V_0}+\frac{\mathcal{M}_s}{Re}\frac{(S(\phi^{n+1})-S_0)^2-(S(\phi^n)-S_0)^2}{2S_0}$$
$$-\frac{\kappa_B}{Re}\int_{\partial\Omega_w}\partial_n f^{n+\frac{1}{2}}(\phi^{n+1}-\phi^n)ds-\frac{\mathcal{M}_s}{Re}\int_{\partial\Omega_w}\frac{S(\phi^{n+\frac{1}{2}})-S_0}{S_0}\epsilon\partial_n\phi^{n+\frac{1}{2}}(\phi^{n+1}-\phi^n)ds\ . \tag{43}$$

Multiplying the third equation in system (33) by $\frac{\mu^{n+\frac{1}{2}}\Delta t}{Re}$ and integration by parts yield

$$\frac{1}{Re}\int_\Omega \mu^{n+\frac{1}{2}}(\phi^{n+1}-\phi^n)d\boldsymbol{x}+\frac{\Delta t}{Re}\int_\Omega \mu^{n+\frac{1}{2}}(\mathbf{u}^{n+\frac{1}{2}}\cdot\nabla)\phi^{n+\frac{1}{2}}d\boldsymbol{x}=-\frac{\mathcal{M}\Delta t}{Re}\int_\Omega(\mu^{n+\frac{1}{2}})^2 d\boldsymbol{x}\ . \tag{44}$$

Multiplying the last equation in system (33) by $\frac{\lambda^{n+\frac{1}{2}}\Delta t}{Re}$ and integration by parts give

$$-\frac{\Delta t}{Re}\int_\Omega \xi\epsilon^2(\phi^n)^2\left|\nabla\lambda^{n+\frac{1}{2}}\right|^2 d\boldsymbol{x}+\frac{\Delta t}{Re}\int_\Omega(\lambda^{n+\frac{1}{2}}\delta_\epsilon\mathcal{P}^n):\nabla\mathbf{u}^{n+\frac{1}{2}}d\boldsymbol{x}=0\ . \tag{45}$$

The discretized energy dissipation law (37) is obtained by combining Eqs. (42)-(45) and organizing the terms according to the boundary conditions $L(\phi)$ as shown in (34). ■

Remark 4.2. *The semi-discrete scheme given by Eq.* (33) *is second-order accurate in time except for the last equation. It can be changed to be second-order accurate as well by using* $\phi^{n+1/2}$ *and* $\mathcal{P}^{n+1/2}$*. However, this change makes the Newton iteration discussed in next session very complicated. For simplicity of computer implementation, a first-order accurate treatment for the last equation is adopted here.*

4.2 Fully-discrete C^0 finite element scheme

The spatial discretization using C^0 finite element is straight forward. Let Ω be the domain of interest with a Lipschitz-continuous boundary $\partial\Omega$. Let ${\mathbf{W}_b}^h \subset \mathbf{W}_b$ be a finite element space with respect to the triangulation of the domain Ω. The fully discrete scheme for Eqs. (23)-(24) is to find

$({\phi_h}^{n+1}, {\mu_h}^{n+1}, {f_h}^{n+1}, {\lambda_h}^{n+1}, {p_h}^{n+1}, {\mathbf{u}_h}^{n+1}) \in {\mathbf{W}_b}^h$, such that for any $(\psi_h, \chi_h, \zeta_h, \Theta_h, q_h, \mathbf{v}_h) \in \mathbf{W}_b^h$,

$$
\begin{cases}
\int_\Omega \left(\frac{\mathbf{u}_h^{n+1}-\mathbf{u}_h^n}{\Delta t} + (\mathbf{u}_h^{n+\frac{1}{2}} \cdot \nabla)\mathbf{u}_h^{n+\frac{1}{2}} + \frac{1}{Re}\nabla P_h^{n+\frac{1}{2}} \right) \cdot \mathbf{v}_h d\boldsymbol{x} = -\int_\Omega \frac{1}{Re}(\eta_h^n(\nabla \mathbf{u}_h^{n+\frac{1}{2}} + (\nabla \mathbf{u}_h^{n+\frac{1}{2}})^T)) : \nabla \mathbf{v}_h d\boldsymbol{x} \\
\qquad + \int_\Omega \frac{1}{Re}\mu_h^{n+\frac{1}{2}} \nabla \phi_h^{n+\frac{1}{2}} \cdot \mathbf{v}_h d\boldsymbol{x} - \int_\Omega \frac{1}{Re}\lambda_h^{n+\frac{1}{2}} \mathcal{P}_h^n \delta_\epsilon : \mathbf{v}_h d\boldsymbol{x} \\
\qquad + \int_{\partial\Omega_w} \frac{1}{Re}\mathbf{n} \cdot (\eta_h^n(\nabla \mathbf{u}_h^{n+\frac{1}{2}} + (\nabla \mathbf{u}_h^{n+\frac{1}{2}})^T) + \lambda_h^{n+\frac{1}{2}} \mathcal{P}_h^n \delta_\epsilon) \cdot \mathbf{v}_h ds \ , \\
\int_\Omega (\nabla \cdot \mathbf{u}_h^{n+\frac{1}{2}}) q_h d\boldsymbol{x} = 0 \ , \\
\int_\Omega (\frac{\phi_h^{n+1}-\phi_h^n}{\Delta t} + (\mathbf{u}_h^{n+\frac{1}{2}} \cdot \nabla)\phi_h^{n+\frac{1}{2}}) \psi_h d\boldsymbol{x} = -\int_\Omega \mathcal{M}\mu_h^{n+\frac{1}{2}} \psi_h d\boldsymbol{x} \ , \\
\int_\Omega \mu_h^{n+\frac{1}{2}} \chi_h d\boldsymbol{x} = \int_\Omega \Bigg(\kappa_B \frac{1}{\epsilon^2}((\phi_h^{n+1})^2 + (\phi_h^n)^2 + \phi_h^{n+1}\phi_h^n - 1) f_h^{n+\frac{1}{2}} + \mathcal{M}_v \frac{(V(\phi_h^{n+\frac{1}{2}}) - V(\phi_0))}{V(\phi_0)} \\
\qquad + \mathcal{M}_s \frac{(S(\phi_h^{n+\frac{1}{2}}) - S(\phi_0))}{S(G_0)} (\frac{1}{4\epsilon}((\phi_h^{n+1})^2 + (\phi_h^n)^2 - 2)(\phi_h^{n+1} + \phi_h^n)) \Bigg) \chi_h d\boldsymbol{x} \\
\qquad + \int_\Omega (\kappa_B \nabla f_h^{n+\frac{1}{2}} + \mathcal{M}_s \epsilon \frac{(S(\phi_h^{n+\frac{1}{2}}) - S(\phi_0))}{S(G_0)} \nabla \phi_h^{n+\frac{1}{2}}) \cdot \nabla \chi_h d\boldsymbol{x} \\
\qquad - \int_{\partial\Omega_w} (\kappa_B \partial_{\mathbf{n}} f_h^{n+\frac{1}{2}} + \mathcal{M}_s \epsilon \frac{(S(\phi_h^{n+\frac{1}{2}}) - S(\phi_0))}{S(G_0)} \partial_{\mathbf{n}} \phi_h^{n+\frac{1}{2}}) \chi_h ds \ , \\
\int_\Omega f_h^{n+\frac{1}{2}} \zeta_h d\boldsymbol{x} = \int_\Omega \epsilon \nabla \phi_h^{n+\frac{1}{2}} \cdot \nabla \zeta_h d\boldsymbol{x} + \int_\Omega \frac{1}{\epsilon}((\phi_h^{n+\frac{1}{2}})^2 - 1)\phi_h^{n+\frac{1}{2}} \zeta_h d\boldsymbol{x} - \int_{\partial\Omega_w} \varepsilon \partial_{\mathbf{n}} \phi_h^{n+\frac{1}{2}} \zeta_h ds \ , \\
-\int_\Omega \xi \epsilon^2 ((\phi_h^n)^2 \nabla \lambda_h^{n+\frac{1}{2}}) \cdot \nabla \Theta_h d\boldsymbol{x} + \int_\Omega \delta_\epsilon \mathcal{P}_h^n : \nabla \mathbf{u}_h^{n+\frac{1}{2}} \Theta_h d\boldsymbol{x} + \int_{\partial\Omega_w} \xi \epsilon^2 ((\phi_h^n)^2 \partial_{\mathbf{n}} \lambda_h^{n+\frac{1}{2}}) \Theta_h ds = 0 \ .
\end{cases}
\tag{46}
$$

Theorem 4.4. *If* $({\phi_h}^{n+1}, {\mu_h}^{n+1}, {f_h}^{n+1}, {\lambda_h}^{n+1}, {p_h}^{n+1}, {\mathbf{u}_h}^{n+1}) \in {\mathbf{W}_b}^h$ *are solutions of the above system, then the following energy law is satisfied:*

$$
\begin{aligned}
\mathcal{E}_{total,h}^{n+1} - \mathcal{E}_{total,h}^n \ = \ & \frac{\triangle t}{Re} \Bigg(-2\|(\eta_h^n)^{1/2} \mathbf{D}_\eta^{n+\frac{1}{2}}\|^2 - \mathcal{M}\|\mu_h^{n+\frac{1}{2}}\|^2 - \xi\| \ \epsilon \phi_h^n \nabla \lambda_h^{n+\frac{1}{2}}\|^2 \\
& - \frac{1}{\kappa}\|L(\phi_h^{n+\frac{1}{2}})\|_w^2 - \|l_s^{-1/2} \mathbf{u}_{\tau,h}^{n+\frac{1}{2}}\|_w^2 \Bigg) \ ,
\end{aligned}
\tag{47}
$$

It is easy to prove this theorem by letting $\mathbf{v}_h = \Delta t \mathbf{u}_h^{n+1}, q_h = \frac{\Delta t p_h^{n+1}}{Re}, \psi_h = \frac{c_h^{n+1} - c_h^n}{Re}, \chi_h = \frac{\Delta t \mu_h^n + 1}{Re}, \Theta_h = \frac{\Delta t \lambda_h^{n+1}}{Re}$ and following the process of proving **Theorem 4.1**.

4.3 Linearization and unique solvability

Note that the energy stable scheme (46) is a coupled nonlinear system. Newton's method [26] is used to solve the equations (46). First, the scheme (46) can be written into the following form:

$$
\mathcal{F}_h^{n+1} = \mathcal{C} \ ,
$$

by relocating all of the constant terms to the right-hand side (RHS) of the equations and the terms contain unknown variables to the left-hand side (LHS), respectively. For the sake of simplification,

we let $\mathbb{U}^{n+1,k} = ({\phi_h}^{n+1,k}, {\mu_h}^{n+1,k}, {f_h}^{n+1,k}, {\lambda_h}^{n+1,k}, {\mathbf{u}_h}^{n+1,k}, {p_h}^{n+1,k})$ be the solution at time $(n+1)\Delta t$ in the k^{th} iteration of Newton's method, and the variations be

$$(\delta\mathbb{U})^{n+1,k} = ((\delta\phi_h)^{n+1,k+1}, (\delta\mu_h)^{n+1,k+1}, (\delta f_h)^{n+1,k+1}, (\delta\lambda_h)^{n+1,k+1}, (\delta\mathbf{u}_h)^{n+1,k+1}, (\delta p_h)^{n+1,k+1}) \ ,$$

where $(\delta\cdot)$ stands for the amount of change of the value, $(\delta\cdot)^{n+1,k} = (\cdot)^{n+1,k+1} - (\cdot)^{n+1,k}$. Newton's method can be formally written as:

$$\mathcal{F}_h^{n+1}(\mathbb{U}^{n+1,k}) + \nabla_{\mathbb{U}^{n+1,k}}\mathcal{F}_h^{n+1} \cdot (\delta\mathbb{U})^{n+1,k} = \mathcal{C}(\mathbb{U}^n) \ .$$

The solution is updated by $\mathbb{U}_h^{n+1,k+1} = \mathbb{U}_h^{n+1,k} + \delta\mathbb{U}_h^{n+1,k}$, where $\mathbb{U}^{n+1,0} = \mathbb{U}^n$. Then we have the following theorem for the solvability.

Theorem 4.5. *If the time step Δt is small enough, then the scheme* (46) *is uniquely solvable.*

Proof: From the last three equations we find $\mu_h^{n+1} = \mu(\phi_h^{n+1})$, $f_h^{n+1} = f(\phi_h^{n+1})$, $\lambda_h^{n+1} = \lambda(\mathbf{u}_h^{n+1})$. With the first and the second equations, P_h^{n+1} can be expressed as $P_h^{n+1} = P(\mathbf{u}_h^{n+1}, \phi_h^{n+1})$. Then the first and the third equations can be solved separately. Applying Newton's method to the first three equations, we have their linearized form:

$$\mathcal{F}(\mathbf{u}_h^{n+1,k}, \phi_h^{n+1,k}) + \nabla_{\mathbf{u}_h^{n+1,k}, \phi_h^{n+1,k}}\mathcal{F}(\mathbf{u}_h^{n+1,k}, \phi_h^{n+1,k}) \cdot (\mathbf{u}_h^{n+1,k+1} - \mathbf{u}_h^{n+1,k}, \phi_h^{n+1,k+1} - \phi_h^{n+1,k})^T = \mathcal{C} \quad (48)$$

Note that $\mathbf{u}_h^{n+1,k+1} = (u_h^{n+1,k}, v_h^{n+1,k+1})$. Multiplying Δt to (48) yields

$$\begin{pmatrix} I - \Delta t A_{11} & \Delta t A_{12} & \Delta t A_{13} \\ \Delta t A_{21} & I - \Delta t A_{22} & \Delta t A_{23} \\ \Delta t A_{31} & \Delta t A_{32} & I - \Delta t A_{33} \end{pmatrix} \begin{pmatrix} u_h^{n+1,k+1} \\ v_h^{n+1,k+1} \\ \phi_h^{n+1,k+1} \end{pmatrix} = \mathcal{C}' \quad (49)$$

where

$A_{11} = \frac{1}{4}(u_h^{n+1,k}\partial_{x,h} + \partial_{x,h}u_h^{n+1,k} + u_h^n\partial_{x,h} + \partial_{x,h}u_h^n + \partial_{y,h}v_h^{n+1,k}) - \frac{1}{2Re}(2\partial_{x,h}(\eta_h^n\partial_{x,h}) + \partial_{y,h}(\eta_h^n\partial_{y,h})) + \frac{1}{2Re}\frac{\partial_h(\partial_{x,h}P_h^{n+1,k})}{\partial_h u_h^{n+1,k}} - \frac{1}{4Re}\frac{\partial_h(\partial_{x,h}(\lambda_h^{n+1,k}(\partial_{x,h}\phi_h^n)^2)) + \partial_{y,h}(\lambda_h^{n+1,k}\partial_{x,h}\phi_h^n\partial_{y,h}\phi_h^n)}{\partial u_h^{n+1,k}}$,

$A_{12} = \frac{1}{4}u_h^{n+1,k}\partial_{y,h} - \frac{1}{2Re}\eta_h^n\partial_{x,h}\partial_{y,h} + \frac{1}{2Re}\frac{\partial_h(\partial_{x,h}P_h^{n+1,k})}{\partial_h v_h^{n+1,k}} - \frac{1}{4Re}\frac{\partial_h(\partial_{x,h}(\lambda_h^{n+1,k}(\partial_{x,h}\phi_h^n)^2)) + \partial_{y,h}(\lambda_h^{n+1,k}\partial_{x,h}\phi_h^n\partial_{y,h}\phi_h^n)}{\partial v_h^{n+1,k}}$,

$A_{13} = -\frac{1}{4Re}(\mu_h^{n+1,k}\partial_{x,h} + \frac{\partial\mu_h^{n+1,k}}{\partial\phi_h^{n+1,k}}\partial_{x,h}\phi_h^{n+1,k} + \mu_h^n\partial_{x,h} + \frac{\partial\mu_h^{n+1,k}}{\partial\phi_h^{n+1,k}}\partial_{x,h}\phi_h^n)$,

$A_{21} = \frac{1}{4}v_h^{n+1,k}\partial_{x,h} - \frac{1}{2Re}\eta_h^n\partial_{x,h}\partial_{y,h} + \frac{1}{2Re}\frac{\partial_h(\partial_{y,h}P_h^{n+1,k})}{\partial_h u_h^{n+1,k}} - \frac{1}{4Re}\frac{\partial_h(\partial_{y,h}(\lambda_h^{n+1,k}(\partial_{y,h}\phi_h^n)^2)) + \partial_{x,h}(\lambda_h^{n+1,k}\partial_{x,h}\phi_h^n\partial_{y,h}\phi_h^n)}{\partial u_h^{n+1,k}}$,

$A_{22} = \frac{1}{4}(v_h^{n+1,k}\partial_{y,h} + \partial_{y,h}v_h^{n+1,k} + v_h^n\partial_{y,h} + \partial_{y,h}v_h^n + \partial_{x,h}u_h^{n+1,k}) - \frac{1}{2Re}(\partial_{x,h}(\eta_h^n\partial_{x,h}) + 2\partial_{y,h}(\eta_h^n\partial_{y,h})) + \frac{1}{2Re}\frac{\partial_h(\partial_{y,h}P_h^{n+1,k})}{\partial_h v_h^{n+1,k}} - \frac{1}{4Re}\frac{\partial_h(\partial_{y,h}(\lambda_h^{n+1,k}(\partial_{y,h}\phi_h^n)^2)) + \partial_{x,h}(\lambda_h^{n+1,k}\partial_{x,h}\phi_h^n\partial_{y,h}\phi_h^n)}{\partial v_h^{n+1,k}}$,

$A_{23} = -\frac{1}{4Re}(\mu_h^{n+1,k}\partial_{y,h} + \frac{\partial\mu_h^{n+1,k}}{\partial\phi_h^{n+1,k}}\partial_{y,h}\phi_h^{n+1,k} + \mu_h^n\partial_{y,h} + \frac{\partial\mu_h^{n+1,k}}{\partial\phi_h^{n+1,k}}\partial_{y,h}\phi_h^n)$,

$A_{31} = \frac{1}{4}\partial_x(\phi_h^{n+1,k} + \phi_h^n)$,

$A_{32} = \frac{1}{4}\partial_y(\phi_h^{n+1,k} + \phi_h^n)$,

$A_{33} = \frac{1}{4}((u_h^{n+1,k} + u_h^n)\partial_{x,h} + (v_h^{n+1,k} + v_h^n)\partial_{y,h}) + \mathcal{M}\frac{\partial\mu_h^{n+1,k}}{\partial\phi_h^{n+1,k}}$.

Using Gaussian elimination, left side of the above matrix system can be transformed as follows

$$\begin{pmatrix} I-\Delta tA_{11} & \Delta tA_{12} & \Delta tA_{13} \\ 0 & I-\Delta tA_{22}-(\Delta t)^2(I-\Delta tA_{11})^{-1}A_{21}A_{12} & \Delta tA_{23}-(\Delta t)^2(I-\Delta tA_{11})^{-1}A_{21}A_{13} \\ 0 & 0 & A'_{33} \end{pmatrix} \quad (50)$$

Where $A'_{33} = I-\Delta tA_{33}-(\Delta t)^2(I-\Delta tA_{22}-(\Delta t)^2(I-\Delta tA_{11})^{-1}A_{21}A_{12})^{-1}A_{32}A_{23}$. C, C' are constant matrices. When Δt is small enough, $I-\Delta tA_{ii}(i=1,2,3)$ is invertible. Thus the given matrix is invertible, we can obtain the unique solution of $(\mathbf{u}_h^{n+1,k+1}, \phi_h^{n+1,k+1})$ with given boundary condition, which means the equation (46) is uniquely solvable. ■

5 Simulation Results

Numerical simulations using the model introduced in the paper are presented in this section. The first example is used to illustrate the convergence and energy stability of the proposed numerical scheme. Then feasibility of the proposed model and the model simulation scheme to studying vesicle motion and shape transformation is assessed by cell tank treading and tumbling tests. The last simulation is devoted to studying effects of mechanical and geometric properties of a vesicle on its deformability when it passes through a narrow channel.

5.1 Convergence study

The initial condition of the convergence test is set to be a 2D tear shape vesicle in a closed cube with intercellular and extracellular fluid velocity being 0. The initial conditions are:

$$\phi_0(x) = \begin{cases} -tanh[(15(y-0.185)(y-0.065)-x+0.125)/\sqrt{2}\varepsilon], & x < 0.125 \\ -tanh[(\sqrt{(x-0.125)^2+(y-0.125)^2}-0.06)/\sqrt{2}\varepsilon], & x >= 0.125, \end{cases} \quad (51)$$
$$\mathbf{u}_0 = (0,0).$$

Thanks to the bending force of the cell membrane, the shape of the vesicle gradually transforms into a perfect circle to minimize the total energy (see Figure 1). The parameter values used for this simulation are chosen as follows: $Re = 2\times10^{-4}$, $\mathcal{M} = 5\times10^{-5}$, $\kappa_B = 8\times10^{-1}$, $\epsilon = 2.5\times10^{-2}$, $\mathcal{M}_v = 20$, $\mathcal{M}_s = 2$, $\xi = 1.6\times10^5$, $\kappa = 8\times10^{-10}$, $\alpha_w = 2\times10^9$, $l_s = 5\times10^{-3}$.

In the simulations, the numerical solution computed with a mesh size $h = 1/240$ is treated as the reference solution or "the true solution". As shown in Table 1, our scheme is a second-order accurate in space.

The time convergence rate of the scheme is obtained by comparing the numerical errors calculated using each pair of successively reduced time step sizes. The purpose of doing so is to eliminate the influence from the error of the reference solution which is also a numerical result. Larger Reynolds number Re and interface thickness ϵ, and a smoother initial profile of the interface are applied to ensure that the convergence rate is not affected by any sharp changes in the phase field label function $\phi(\boldsymbol{x})$. Results in Table 2 confirm that our scheme is a also second-order accurate in time.

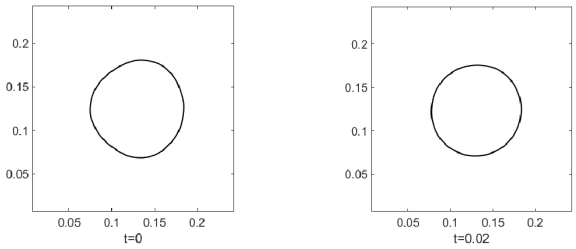

Figure 1: Relaxation of a tear shape vesicle.

Spacial mesh size h	P2 Element					
	Err(u_x)	Convergence Rate(u_x)	Err(u_y)	Convergence Rate(u_y)	Err(ϕ)	Convergence Rate(ϕ)
1/47	1.3e-1		1.5e-1		1.4e-2	
1/71	8.3e-2	1.15	7.6e-2	1.71	6.1e-3	1.97
1/107	3.8e-2	1.94	3.7e-2	1.83	2.3e-3	2.45
1/160	1.5e-2	2.35	1.3e-2	2.59	5.7e-4	3.42

Table 1: L^2 norm of the error and convergence rate for velocity $\mathbf{u} = (u_x, u_y)$, phase-field function ϕ, at time $t = 0.02$ with both intercellular and extracellular fluid viscosity being 1.

Remark 5.1. *During the convergence test, we mainly focus on the convergence rates of the velocity and the phase-field function. The local inextensibility is neglected, and only the global area and volume constraints are taken into consideration.*

Finally, the energy law (**Theorem 4.1**) and conservation of mass and surface area of vesicles are tested by simulating the relaxation of a bent vesicle. The vesicle gradually evolves back to its equilibrium biconcave shape. Figure 2 shows the snapshots of the vesicle profile at different times $t = 0, 0.25, 0.5$ and 1.25. The parameter values used here are:

$Re = 2 \times 10^{-4}$, $\mathcal{M} = 2.5 \times 10^{-3}$, $\kappa_B = 2$, $\epsilon = 7.5 \times 10^{-3}$, $\mathcal{M}_v = 20$, $\mathcal{M}_s = 2$, $\xi = 7.1 \times 10^4$, $\kappa = 2 \times 10^{-10}$, $\alpha_w = 2 \times 10^9$, $l_s = 0.5$.

The initial conditions are:

$$\phi_0(x) = \begin{cases} -tanh[(5(y-0.7)(y-0.3) - x + 0.5)/\sqrt{2}\varepsilon], & x < 0.5 \\ -tanh[(400(y-0.7)(y-0.3)(y-0.5)^2 + x - 0.5)/\sqrt{2}\varepsilon], & x >= 0.5, \end{cases} \tag{52}$$

$\mathbf{u}_0 = (0, 0)$.

The changes of vesicle mass and surface area and the change of total discrete energy of this test case computed by the scheme (Eqs. (23)-(24)) are shown in Figure 3. It is evident that the vesicle mass and surface area are almost perfectly preserved, and the total energy decays over the course of time as expected.

time step Δt	P2 Element					
	Err(u_x)	Convergence Rate(u_x)	Err(u_y)	Convergence Rate(u_y)	Err(ϕ)	Convergence Rate(ϕ)
0.025	-		-		-	
0.0125	8.12e-6		8.13e-6		9.92e-6	
0.00625	2.90e-6	1.49	2.97e-6	1.45	2.42e-6	2.04
0.003125	1.03e-6	1.48	1.07e-6	1.48	5.98e-7	2.01
0.0015625	2.53e-7	2.03	2.60e-7	2.03	1.49e-7	2.01

Table 2: L^2 norm of the error and convergence rate for velocity $\mathbf{u} = (u_x, u_y)$, phase-field function ϕ, at time $t = 0.05$ with both intercellular and extracellular fluid viscosities being 1.

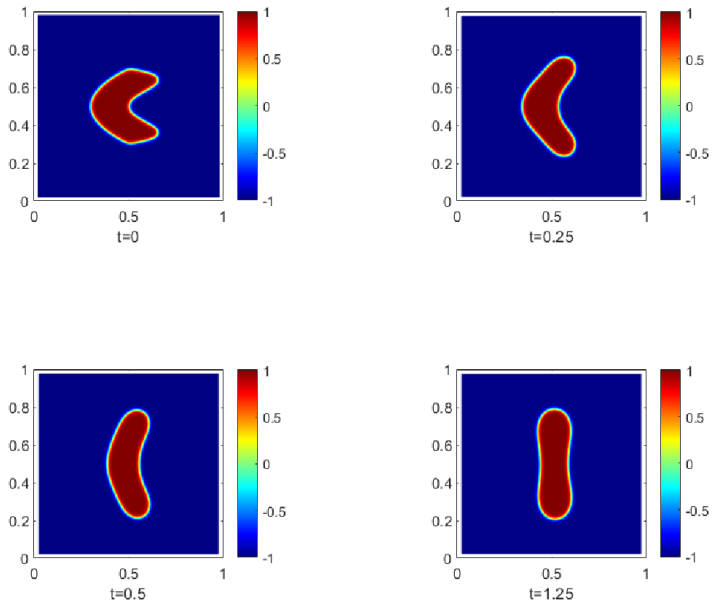

Figure 2: Relaxation of a bent vesicle. The fluid viscosities are 1 and 50 for intercellular and extracellular fluids, respecfively.

5.2 Tank treading and tumbling

The vesicle motion in a Couette flow changes with respect to the ratio of the viscosities η_{in} and η_{out} of intracellular and extracellular fluids [38, 4, 21, 30]. When this viscosity ratio is small, the vesicle is prone to move in the tank treading mode; while the tumbling mode is preferred when the viscosity ratio is large. The parameter values utilized for this vesicle motion simulation are set as follows:

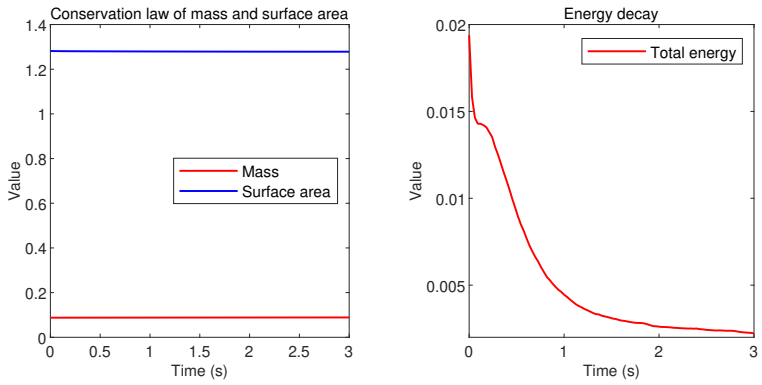

Figure 3: The test case of relaxation of a bent vesicle. Left: Change of mass and surface area vs. time; Right: Change of discrete energy vs. time.

$Re = 2 \times 10^{-4}$, $\delta_\epsilon = |\nabla \phi^n|^2$, $\mathcal{M} = 10^{-3}$, $\kappa_B = 5 \times 10^{-3}$, $\epsilon = 7.5 \times 10^{-3}$, $\mathcal{M}_v = 20$, $\mathcal{M}_s = 200$, $\xi = 1.78 \times 10^7$, $\kappa = 2 \times 10^{-12}$, $\alpha_w = 2 \times 10^9$, $l_s = 0.2$.

The upper and bottom walls of the domain are set to move in opposite direction horizontally with velocities -20 and 20, respectively. The simulation domain is 2×1, and the initial shape of the vesicle is chosen to be an ellipse with eccentricity $\sqrt{3}$. The ratios of viscosities of the intracellular and extracellular fluids are set to be $1:1$ and $1:500$, respectively. Figures 4 and 5 show the interfaces of tank treading vesicle (low viscosity ratio case) and tumbling vesicle (high viscosity ratio case) and corresponding fluid velocity fields at different times, respectively. A point on the interface (black solid) is tracked to illustrate these two different types of motion. For the tank treading motion, the angle between the long axis of the vesicle and horizontal axis is fixed when the vesicle is at equilibrium, but the tracer point rotates in a counter clockwise direction along the membrane. For the tumbling motion, the vesicle keeps rotating and the tracer point does not move with respect to the membrane shape.

Remark 5.2. *Tracking of the marker point (the black solid dot) is done by the following steps:*

1. *Determine a marker point P that is located on the interface with coordinate (x, y);*
2. *Compute the velocity $\mathbf{u}(P) = (u_x(P), u_y(P))$ of the marker point by interpolation;*
3. *Update the marker point position at the next time point by $(x + u_x(P)\Delta t, y + u_y(P)\Delta t)$;*
4. *Go to step 2.*

This tracking gives the trajectory of the marker point.

Next, simulation result of tumbling motion of a rigid ellipse is compared with the theoretical solution obtained using Jeffery's orbit theory [34]. Specifically, the angle between the long axis of the ellipse and the horizontal axis is compared. As shown in Figure 6, our simulation result is in close agreement with the analytical Jeffery orbit.

Remark 5.3. *The long axis of the rigid ellipse during the tumbling motion is determined as follows:*

1. *Determine the interface location of the ellipse by $\phi = 0$;*
2. *Find the point on the interface that is farthest away from the center of the vesicle in upper domain;*
3. *Match these two points and the line is considered as the long axis of the ellipse.*

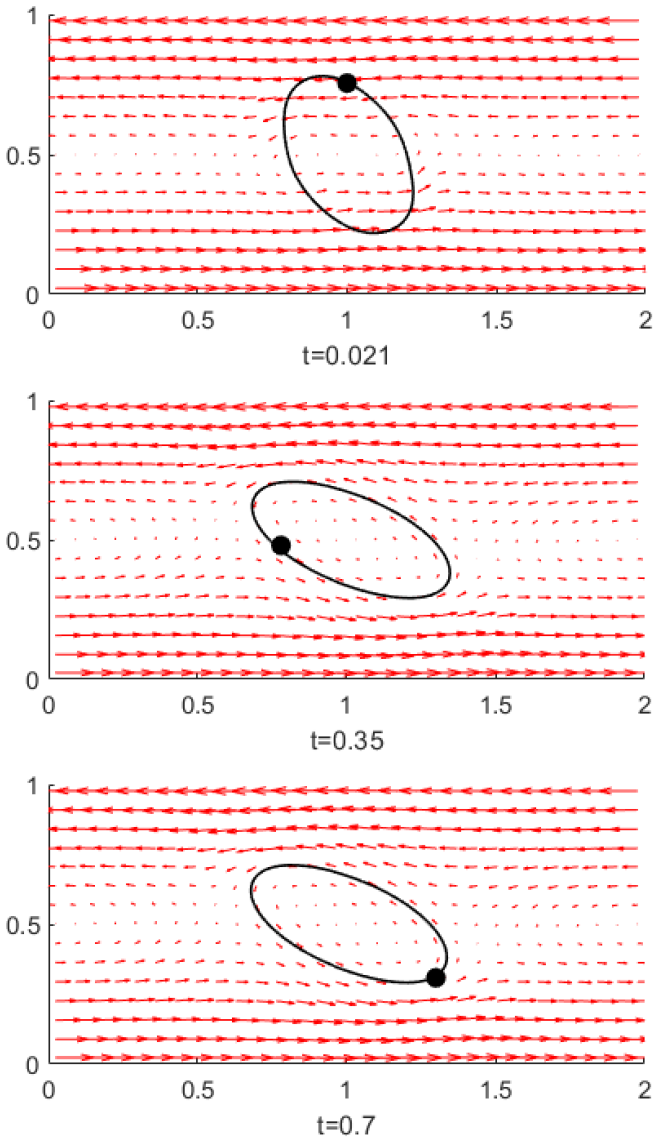

Figure 4: Tank treading with viscosity ratio 1 : 1. The orientation of the vesicle and the velocity field are kept stable when the system comes to equilibrium. The tracer point (in black) on the membrane rotates in the clockwise direction along the vesicle.

Since the ellipse is located at the center of the domain at the initial time point, and the motion of the fluid is centrosymmetric according to the specified boundary condition, it is expected that the center of the ellipse is kept at the center of the domain Ω. Therefore the determination of the long axis of the ellipse based on its geometry character is acceptable.

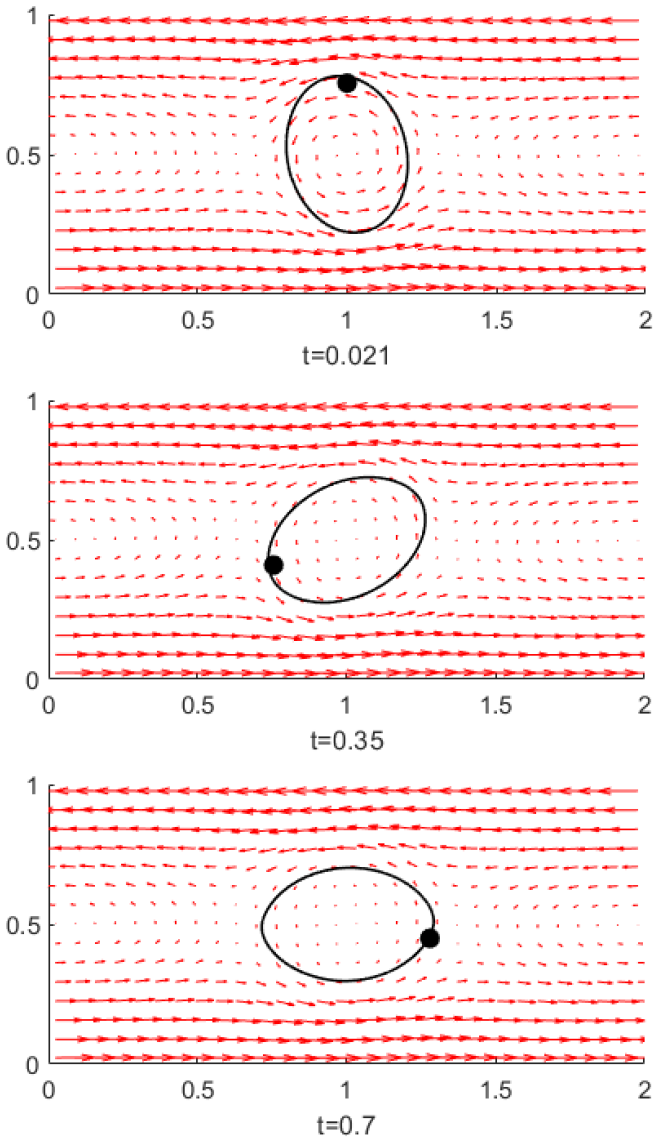

Figure 5: Tumbling with viscosity ratio 1:500. The vesicle keeps rotating in the flow. Position of the tracer point (in black) is fixed with respect to the vesicle membrane.

5.3 Vesicle passing through a narrow fluid channel

Finally, the calibrated model is used to study the effects of mechanical properties of the membrane of the vesicle on its circulating through constricting micro channels [29]. The vesicle shape is described by an ellipse with eccentricity $\sqrt{3}$, and the width of the squeezing section of the narrow channel is 0.3 by default. A pressure drop boundary condition is applied at the inlet(left) and outlet(right) of the domain by setting the pressure on the inlet and outlet to be $P = 50$ and $P = -50$, respectively. Fluid viscosity ratio is set to be $1 : 10$ for extracellular and intracellular fluids, respectively. The other parameters are as follows:

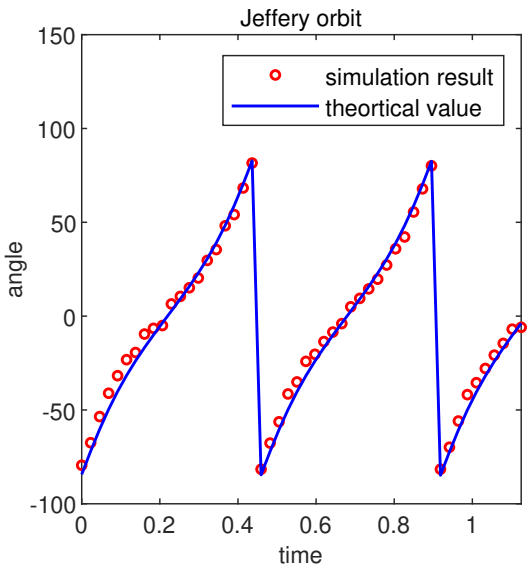

Figure 6: Comparison between theoretical and simulation results of the flipping ellipse. The blue line is the angle between the long axis of the ellipse and the horizontal axis predicted by the Jeffery orbit theory, and the red circles are the angle from the simulation.

$Re = 2 \times 10^{-4}$, $\delta_\epsilon = 10 \times |\nabla \phi^n|^2$, $\mathcal{M} = 5 \times 10^{-4}$, $\kappa_B = 4 \times 10^{-2}$, $\epsilon = 7.5 \times 10^{-3}$, $\mathcal{M}_v = 20$, $\mathcal{M}_s = 100$, $\xi = 7.1 \times 10^4$, $\kappa = 4 \times 10^{-11}$, $\alpha_w = 2 \times 10^9$, $l_s = 5 \times 10^{-3}$.

Effect of the local inextensibility of vesicle membrane is assessed by comparing vesicle simulations with and without using the local inextensibility constraint $\mathcal{P} : \nabla \mathbf{u} = 0$ in the model. Snapshots of these simulations at different times are shown in Figure 7. They illustrate that a vesicle modeled without using the local inextensiblity can pass through the channel by introducing large extension and deformation of its body with a relatively small value of global inextensibility coefficient $\mathcal{M}_s$; while a vesicle modeled with the local inextensibility hardly exhibits large extension and deformation of its body and blocks the channel. This is also confirmed by Figure 8. It shows under otherwise same conditions, the total arc length of the membrane of the vesicle modeled without the local inextensibility increases significantly when it passes through the channel, and the vesicle with the local inextensibilty preserves its membrane arc length well during the course of the simulation.

Although the total arc length of a vesicle without the local inextensibility and with a very large $\mathcal{M}_s$ value could maintain almost unchanged as shown in 7 (c) and 8, the morphological changes of vesicles with and without the local inextensibility are drastically different. For the vesicles modeled without the local inextensibility, Figure 9(b,c) illustrates that the vesicle membranes are stretched (red) or compressed (blue) everywhere, even though the total arc length of the vesicle modeled using a large modulus $\mathcal{M}_s$ value could be preserved, and the vesicle forms the blockage. For the vesicle modeled with the local inextensibility, Figure 9(c) confirms that there is almost no local extension or compression of the membrane, which is consistent with experimental observations. All simulations described below use the local inextensibility.

Both experiments and clinic reports have shown that the cell bending modulus and surface-volume ratio play important roles in determining the deformability of vesicles, especially when

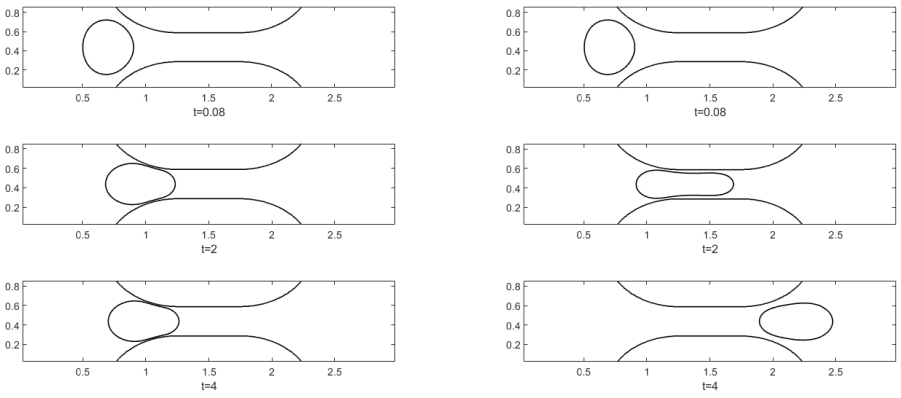

(a) (b)

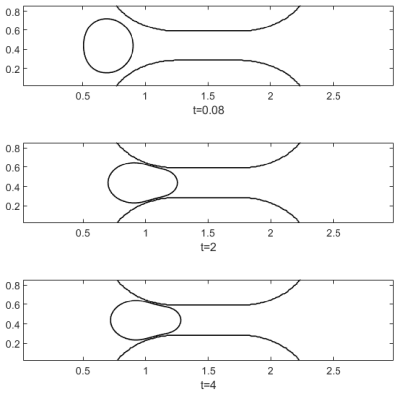

(c)

Figure 7: Snapshots of vesicles passing a narrowed channel with different surface area constraints at times $t = 0.08, 2$ and 4, respectively. (a) $\mathcal{M}_s = 100$ with the local inextensibility; (b) $\mathcal{M}_s = 100$ without the local inextensibility; (c) $\mathcal{M}_s = 20000$ without the local inextensibility. The curves on the top and bottom ceiling are the wall boundary of the narrowed channel.

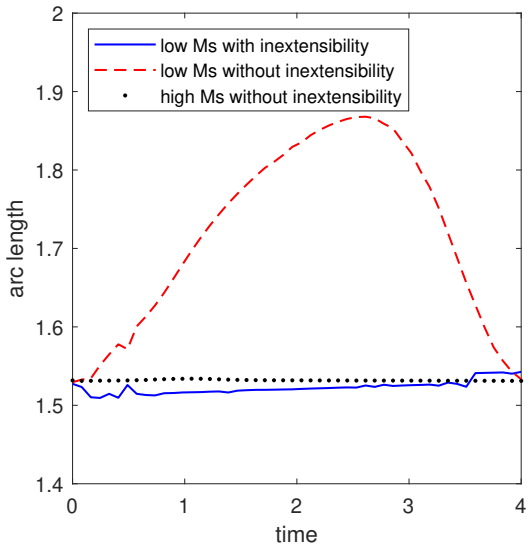

Figure 8: Total arc length of vesicle membrane with the local inextensibility (blue line), and the total arc lengths of vesicle membranes with low (100) (red dashed line) and high (20000) (black point) $\mathcal{M}_s$ and no local inextensibility, respectively, during vesicles passing through the constriction of the micro channel with otherwise same parameter values and settings.

they pass through narrow channels [63, 45, 57]. The latest results reveal that a moderate decrease in the surface-volume ratio has a more significant effect than varying the cell bending stiffness. This surface-volume ratio effect is tested by increasing the ratio value slightly from $1.5 : 1$ to $2 : 1$. Results in Figures 10 and 11 confirm that the more rounded vesicles are much harder to pass through the narrow channel and can easily form the blockage. This is consistent with the experimental observations.

The effect of the bending modulus is assessed by increasing its value 10 times. The surface-volume ratio of the vesicle is $2 : 1$ in this test. Figure 11 illustrates that this more rigid vesicle can also pass the same size channel but exhibits very different shape transformation.

6 Conclusion

In this paper, an energy variational method is used to derive a thermodynamically consistent phase-field model for simulating vesicles motion and deformation under flow conditions. Corresponding Allen-Cahn GNBC boundary conditions accounting for the vesicle-wall (or fluid-structure) interaction are also proposed by introducing the boundary dissipation and the vesicle-wall interaction energy.

Then an efficient C^0 finite element method combined with the mid-point temporal discretization is proposed to solve the obtained model equations. Thanks to the mid-point temporal discretization, the obtained numerical scheme is unconditionally energy stable. The numerical experiments confirm that this scheme is second-order accurate in both space and time. Simulations of the vesicle tank treading and tumbling motions reproduce experimental observations. And the flipping ellipse

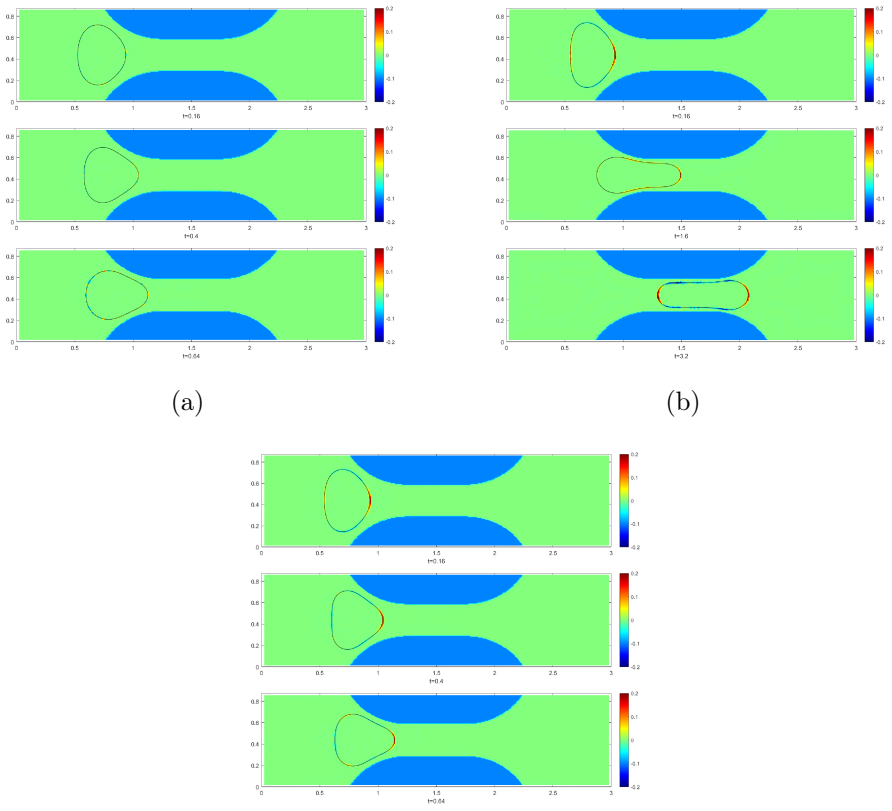

Figure 9: Effects of the local inextensibility $\mathcal{P} : \nabla \mathbf{u} = 0$. Snapshots of membrane forces of vesicles: (a) $\mathcal{M}_s = 100$ with the local inextensibility; (b) $\mathcal{M}_s = 100$ without the local inextensibility; and (c) $\mathcal{M}_s = 20000$ without the local inextensibility.

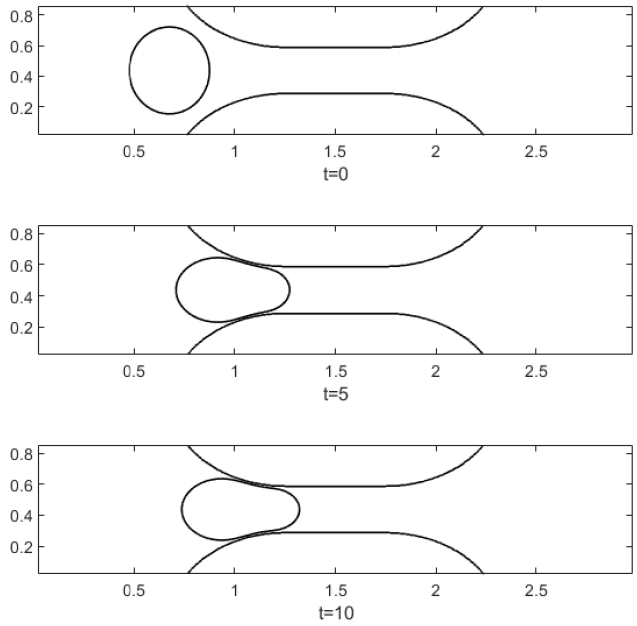

Figure 10: Side view of a vesicle with surface-volume ratio 1.5 : 1 at different times.

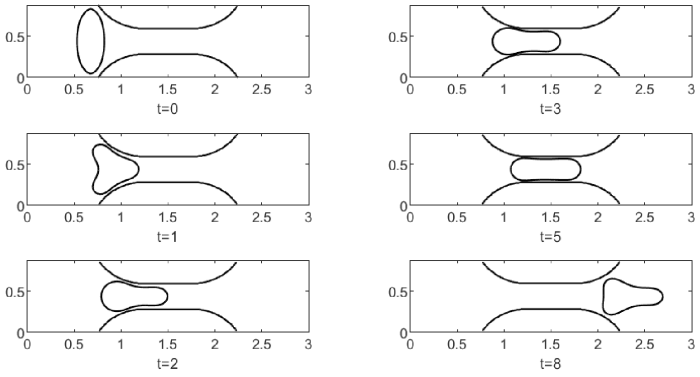

Figure 11: Side view of a vesicle with surface-volume ratio 2 : 1 at different times.

simulation agrees with the analytical solution well. Finally, the model is used to investigate how vesicles' mechanical properties affect the vesicles' capability to pass through narrow channels. It is shown that whether a vesicle can pass a narrow channel is largely determined by the surface-volume ratio of the vesicle, which is consistent with *in vitro* experiments.

Our model can be used to study the effects of mechanical properties of membranes induced by sickle cell disease [3] and diabetes [43]. Combining with the restricted diffusion model [54], our model could be generalized to model the mass transfer through a semi-permeable membrane, like oxygen delivering [65]. Also, with detailed cell-wall and cell-cell interactions submodels, our work is applicable for blood clotting modelling [73, 75] and cell crawling [59].

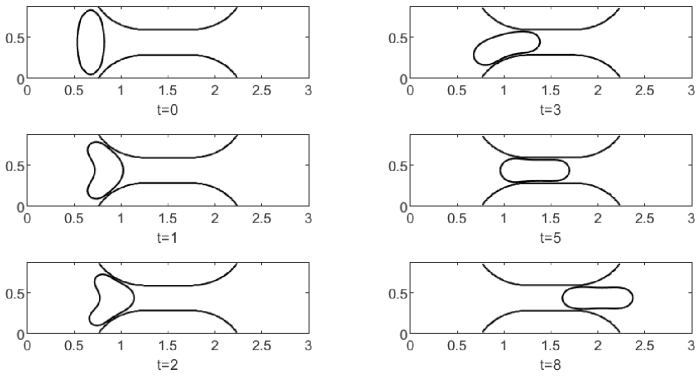

Figure 12: Side view of a vesicle with large bending modulus $\kappa_B = 4 \times 10^{-1}$ and surface-volume ratio $2:1$ at different times.

Authors' contributions

L.S, Z.X, and S.X did the model derivations. L.S, P.L and S.X carried out the numerical analysis and simulations. Z.X, H.H, P.L and S.X designed and coordinated the study. All participated in the preparation of the manuscript. All authors gave final approval for publication.

Declaration of competing interest

The authors declare that they have no known competing financial interests or personal relationships that could have appeared to influence the work reported in this paper.

Acknowledgements

This work was partially supported by the NSFC (grant numbers 12071190, 11771040, 11861131004, 91430106), and NSERC (CA). L.S was partially supported by the Chinese Scholarship Council for studying at the University of Dundee. Z.X was partially supported by the NSF CDS&E-MSS 1854779 and NSF-1821242.

Appendix

The detail of the derivation of the discrete energy law is given: Multiplying the first equation in system (33) by $\Delta t \mathbf{u}^{n+\frac{1}{2}}$ and do integration by parts gives

$$\begin{aligned} & RHS \\ = & \int_\Omega \frac{1}{2}((\mathbf{u}^{n+1})^2 - (\mathbf{u}^n)^2) d\boldsymbol{x} + \int_\Omega \Delta t \mathbf{u}^{n+\frac{1}{2}} \cdot \nabla(\frac{1}{2}|\mathbf{u}^{n+\frac{1}{2}}|^2) d\boldsymbol{x} \\ & -\frac{\Delta t}{Re}\int_\Omega P^{n+\frac{1}{2}} \nabla \cdot \mathbf{u}^{n+\frac{1}{2}} d\boldsymbol{x} + \frac{\Delta t}{Re}\int_{\Omega_w} P^{n+\frac{1}{2}} \mathbf{u}^{n+\frac{1}{2}} \cdot \mathbf{n} ds \end{aligned}$$

$$
\begin{aligned}
&= \int_\Omega \frac{1}{2}((\mathbf{u}^{n+1})^2 - (\mathbf{u}^n)^2)d\boldsymbol{x} - \int_\Omega \Delta t \nabla\cdot\mathbf{u}^{n+\frac{1}{2}}(\frac{1}{2}|\mathbf{u}^{n+\frac{1}{2}}|^2)d\boldsymbol{x} + \int_{\Omega_w}\Delta t\mathbf{u}^{n+\frac{1}{2}}\cdot\mathbf{n}(\frac{1}{2}|\mathbf{u}^{n+\frac{1}{2}}|^2)ds \\
&\quad -\frac{\Delta t}{Re}\int_\Omega P^{n+\frac{1}{2}}\nabla\cdot\mathbf{u}^{n+\frac{1}{2}}d\boldsymbol{x} + \frac{\Delta t}{Re}\int_{\Omega_w} P^{n+\frac{1}{2}}\mathbf{u}^{n+\frac{1}{2}}\cdot\mathbf{n}ds \\
&\quad LHS \\
&= -\frac{\Delta t}{Re}\int_\Omega \nabla\mathbf{u}^{n+\frac{1}{2}} : \eta^n(\nabla\mathbf{u}^{n+\frac{1}{2}} + (\nabla\mathbf{u}^{n+\frac{1}{2}})^T)d\boldsymbol{x} + \frac{\Delta t}{Re}\int_\Omega \mathbf{u}^{n+\frac{1}{2}}\cdot\nabla\phi^{n+\frac{1}{2}}\mu^{n+\frac{1}{2}}d\boldsymbol{x} \\
&\quad -\frac{\Delta t}{Re}\int_\Omega \lambda^{n+\frac{1}{2}}\delta_\epsilon\mathcal{P}^n : \nabla\mathbf{u}^{n+\frac{1}{2}}d\boldsymbol{x} + \frac{\Delta t}{Re}\int_{\partial\Omega_w}\lambda^{n+\frac{1}{2}}(\delta_\epsilon\mathcal{P}^n\cdot\mathbf{n})\cdot\mathbf{u}_\tau^{n+\frac{1}{2}}ds \\
&\quad +\frac{\Delta t}{Re}\int_{\partial\Omega_w}\mathbf{u}^{n+\frac{1}{2}}\cdot\eta^n((\nabla\mathbf{u}^{n+\frac{1}{2}} + (\nabla\mathbf{u}^{n+\frac{1}{2}})^T)\cdot\boldsymbol{n})ds\ . \qquad (53)
\end{aligned}
$$

With the boundary condition $\mathbf{u}^{n+\frac{1}{2}}\cdot\mathbf{n} = 0$ and the constrain$\nabla\cdot\mathbf{u}^{n+\frac{1}{2}} = 0$, we have

$$
RHS \quad = \int_\Omega \frac{1}{2}((\mathbf{u}^{n+1})^2 - (\mathbf{u}^n)^2)d\boldsymbol{x} \qquad (54)
$$

thus we have

$$
\begin{aligned}
&\int_\Omega \frac{1}{2}((\mathbf{u}^{n+1})^2 - (\mathbf{u}^n)^2)d\boldsymbol{x} \\
&= -\frac{\Delta t}{Re}\int_\Omega \nabla\mathbf{u}^{n+\frac{1}{2}} : \eta^n(\nabla\mathbf{u}^{n+\frac{1}{2}} + (\nabla\mathbf{u}^{n+\frac{1}{2}})^T)d\boldsymbol{x} + \frac{\Delta t}{Re}\int_\Omega \mathbf{u}^{n+\frac{1}{2}}\cdot\nabla\phi^{n+\frac{1}{2}}\mu^{n+\frac{1}{2}}d\boldsymbol{x} \\
&-\frac{\Delta t}{Re}\int_\Omega \lambda^{n+\frac{1}{2}}\delta_\epsilon\mathcal{P}^n : \nabla\mathbf{u}^{n+\frac{1}{2}}d\boldsymbol{x} + \frac{\Delta t}{Re}\int_{\partial\Omega_w}\lambda^{n+\frac{1}{2}}(\delta_\epsilon\mathcal{P}^n\cdot\mathbf{n})\cdot\mathbf{u}_\tau^{n+\frac{1}{2}}ds \\
&+\frac{\Delta t}{Re}\int_{\partial\Omega_w}\mathbf{u}^{n+\frac{1}{2}}\cdot\eta^n((\nabla\mathbf{u}^{n+\frac{1}{2}} + (\nabla\mathbf{u}^{n+\frac{1}{2}})^T)\cdot\boldsymbol{n})ds\ . \qquad (55)
\end{aligned}
$$

Multiplying the third equation in system (33) by $\frac{\mu^{n+\frac{1}{2}}\Delta t}{Re}$ and do integration yield

$$
\frac{1}{Re}\int_\Omega \mu^{n+\frac{1}{2}}(\phi^{n+1}-\phi^n)d\boldsymbol{x} + \frac{\Delta t}{Re}\int_\Omega \mu^{n+\frac{1}{2}}(\mathbf{u}^{n+\frac{1}{2}}\cdot\nabla)\phi^{n+\frac{1}{2}}d\boldsymbol{x} = -\frac{\mathcal{M}\Delta t}{Re}\int_\Omega(\mu^{n+\frac{1}{2}})^2 d\boldsymbol{x}\ . \qquad (56)
$$

Multiplying the fourth equation in system (33) by $\frac{\phi^{n+1}-\phi^n}{Re}$ and integration by parts lead to

$$
LHS = \frac{1}{Re}\int_\Omega \mu^{n+\frac{1}{2}}(\phi^{n+1}-\phi^n)d\boldsymbol{x} \qquad (57)
$$

with (4.2) and (4.3) we have the following result on the right hand side:

$$
\begin{aligned}
&\frac{\kappa_B}{2Re}\int_\Omega g(\phi^{n+1},\phi^n)(\phi^{n+1}-\phi^n)d\boldsymbol{x} \\
&= -\frac{\kappa_B}{2Re\varepsilon}\int_\Omega (f^{n+1})^2 - (f^n)^2 d\boldsymbol{x} + \frac{\kappa_B}{Re}\int_{\Omega_w}\partial_n f^{n+\frac{1}{2}}(\phi^{n+1}-\phi^n)ds
\end{aligned}
$$

$$
\begin{aligned}
&\frac{\mathcal{M}_s}{Re}\frac{S(\phi^{n+\frac{1}{2}})-S(\phi_0)}{S(\phi_0)}\int_\Omega f(\phi^{n+1},\phi^n)(\phi^{n+1}-\phi^n)d\boldsymbol{x}\\
&=\frac{\mathcal{M}_s}{Re}\frac{S(\phi^{n+1})+S(\phi^n)-2S(\phi_0)}{2S(\phi_0)}(S(\phi^{n+1})-S(\phi^n))\\
&-\frac{\mathcal{M}_s}{Re}\frac{S(\phi^{n+1})+S(\phi^n)-2S(\phi_0)}{2S(\phi_0)}\int_{\Omega_w}\varepsilon\partial_n\phi^{n+\frac{1}{2}}(\phi^{n+1}-phi^n)ds\\
&=\frac{\mathcal{M}_s}{Re}\frac{S(\phi^{n+1})^2-S(\phi^n)^2-2S(\phi_0)S(\phi^{n+1})+2S(\phi_0)S(\phi^n)+S(\phi_0)^2-S(\phi_0)^2}{2S(\phi_0)}\\
&-\frac{\mathcal{M}_s}{Re}\frac{S(\phi^{n+1})+S(\phi^n)-2S(\phi_0)}{2S(\phi_0)}\int_{\Omega_w}\varepsilon\partial_n\phi^{n+\frac{1}{2}}(\phi^{n+1}-phi^n)ds\\
&=\frac{\mathcal{M}_s}{Re}\frac{(S(\phi^{n+1})-S(\phi_0))^2-(S(\phi^n)-S(\phi_0))^2}{2S(\phi_0)}\\
&-\frac{\mathcal{M}_s}{Re}\frac{S(\phi^{n+1})+S(\phi^n)-2S(\phi_0)}{2S(\phi_0)}\int_{\Omega_w}\varepsilon\partial_n\phi^{n+\frac{1}{2}}(\phi^{n+1}-phi^n)ds
\end{aligned}
\tag{58}
$$

By simple calculation we also have

$$
\begin{aligned}
&\frac{\mathcal{M}_v}{Re}\frac{V(\phi^{n+\frac{1}{2}})-V(\phi_0)}{V_0}\int_\Omega(\phi^{n+1}-phi^n)d\boldsymbol{x}\\
&=\frac{\mathcal{M}_v}{Re}\frac{V(\phi^{n+1})+V(\phi^n)-2V(\phi_0)}{2V(\phi_0)}(V(\phi^{n+1})-V(\phi^n))\\
&=\frac{\mathcal{M}_v}{Re}\frac{V(\phi^{n+1})^2-V(\phi^n)^-2V(\phi_0)V(\phi^{n+1})+2V(\phi_0)V(\phi^n)+V(\phi_0)^2-V(\phi_0)^2}{2V(\phi_0)}\\
&=\frac{\mathcal{M}_v}{Re}\frac{(V(\phi^{n+1})-V(\phi_0))^2-(V(\phi^n)-V(\phi_0))^2}{2V(\phi_0)}
\end{aligned}
\tag{59}
$$

Thus we have the equation

$$
\begin{aligned}
&\frac{1}{Re}\int_\Omega\mu^{n+\frac{1}{2}}(\phi^{n+1}-\phi^n)d\boldsymbol{x}\\
&=-\frac{\kappa_B}{2Re\varepsilon}\int_\Omega(f^{n+1})^2-(f^n)^2d\boldsymbol{x}+\frac{\kappa_B}{Re}\int_{\Omega_w}\partial_n f^{n+\frac{1}{2}}(\phi^{n+1}-\phi^n)ds\\
&+\frac{\mathcal{M}_s}{Re}\frac{(S(\phi^{n+1})-S(\phi_0))^2-(S(\phi^n)-S(\phi_0))^2}{2S(\phi_0)}\\
&-\frac{\mathcal{M}_s}{Re}\frac{S(\phi^{n+1})+S(\phi^n)-2S(\phi_0)}{2S(\phi_0)}\int_{\Omega_w}\varepsilon\partial_n\phi^{n+\frac{1}{2}}(\phi^{n+1}-\phi^n)ds\\
&+\frac{\mathcal{M}_v}{Re}\frac{(V(\phi^{n+1})-V(\phi_0))^2-(V(\phi^n)-V(\phi_0))^2}{2V(\phi_0)}
\end{aligned}
\tag{60}
$$

Where ϕ_0 is the initial condition of phase order. $V(\phi^n)=\int_\Omega\phi^n d\boldsymbol{x}, S(\phi^n)=\int_\Omega\frac{\varepsilon}{2}|\nabla\phi^n|^2+\frac{1}{4\varepsilon}((\phi^n)^2-1)^2d\boldsymbol{x}$. $V(\phi^{n+\frac{1}{2}})=\frac{1}{2}(V(\phi^n+1)+V(phi^n)), S(\phi^{n+\frac{1}{2}})=\frac{1}{2}(S(\phi^n+1)+S(\phi^n))$ are considered as constants in the integration.

Multiplying the last equation in system (33) by $\frac{\lambda^{n+\frac{1}{2}}\Delta t}{Re}$ and integration by parts give

$$-\frac{\Delta t}{Re}\int_\Omega \xi\epsilon^2(\phi^n)^2\left|\nabla\lambda^{n+\frac{1}{2}}\right|^2 d\boldsymbol{x}+\frac{\Delta t}{Re}\int_{\Omega_w}\xi\epsilon^2(\phi^n)^2\lambda^{n+\frac{1}{2}}\partial_n\lambda^{n+\frac{1}{2}}ds+\frac{\Delta t}{Re}\int_\Omega(\lambda^{n+\frac{1}{2}}\delta_\epsilon\mathcal{P}^n):\nabla\mathbf{u}^{n+\frac{1}{2}}d\boldsymbol{x}=0 \quad (61)$$

With the boundary condition $\partial_n\lambda^{n+\frac{1}{2}}=0$, we have

$$-\frac{\Delta t}{Re}\int_\Omega \xi\epsilon^2(\phi^n)^2\left|\nabla\lambda^{n+\frac{1}{2}}\right|^2 d\boldsymbol{x}+\frac{\Delta t}{Re}\int_\Omega(\lambda^{n+\frac{1}{2}}\delta_\epsilon\mathcal{P}^n):\nabla\mathbf{u}^{n+\frac{1}{2}}d\boldsymbol{x}=0\ . \quad (62)$$

(55)-(56)+(60)-(62) and relocate some terms we have

$$\begin{aligned}
&\frac{1}{2}(||\mathbf{u}^{n+1}||^2-||\mathbf{u}^n||^2)+\frac{\kappa_B}{2Re\varepsilon}(||f^{n+1}||^2-||f^n||^2)\\
&+\frac{\mathcal{M}_s}{Re}\frac{(S(\phi^{n+1})-S(\phi_0))^2-(S(\phi^n)-S(\phi_0))^2}{2S(\phi_0)}+\frac{\mathcal{M}_v}{Re}\frac{(V(\phi^{n+1})-V(\phi_0))^2-(V(\phi^n)-V(\phi_0))^2}{2V(\phi_0)}\\
&=-\frac{2\Delta t}{Re}||(\eta^n)^{\frac{1}{2}}D_\eta^{n+\frac{1}{2}}||^2-\frac{\mathcal{M}\Delta t}{Re}||\mu^{n+\frac{1}{2}}||^2-\frac{\Delta t}{Re}\xi||\epsilon(\phi^n)\nabla\lambda^{n+\frac{1}{2}}||^2\\
&+\frac{\Delta t}{Re}\int_{\partial\Omega_w}\mathbf{u}^{n+\frac{1}{2}}\cdot\eta^n((\nabla\mathbf{u}^{n+\frac{1}{2}}+(\nabla\mathbf{u}^{n+\frac{1}{2}})^T)\cdot\boldsymbol{n})ds+\frac{\Delta t}{Re}\int_{\partial\Omega_w}\lambda^{n+\frac{1}{2}}(\delta_\epsilon\mathcal{P}^n\cdot\mathbf{n})\cdot\mathbf{u}_\tau^{n+\frac{1}{2}}ds\\
&+\frac{\mathcal{M}_s}{Re}\frac{S(\phi^{n+1})+S(\phi^n)-2S(\phi_0)}{2S(\phi_0)}\int_{\Omega_w}\varepsilon\partial_n\phi^{n+\frac{1}{2}}(\phi^{n+1}-phi^n)ds+\frac{\kappa_B}{Re}\int_{\Omega_w}\partial_n f^{n+\frac{1}{2}}(\phi^{n+1}-\phi^n)ds \quad (63)
\end{aligned}$$

With boundary conditions: on $\partial\Omega_w$

$$\kappa\dot{\phi}^{n+\frac{1}{2}}=-L^{n+\frac{1}{2}}\ , \quad (64)$$

$$L^{n+\frac{1}{2}}=\kappa_B\partial_n f^{n+\frac{1}{2}}+\mathcal{M}_s\epsilon\frac{S(\phi^{n+\frac{1}{2}})-S_0}{S_0}\partial_n\phi^{n+\frac{1}{2}}+\alpha_w\frac{f_w^{n+1}-f_w^n}{\phi^{n+1}-\phi^n}\ , \quad (65)$$

$$-l_s^{-1}u_{\tau_i}^{n+\frac{1}{2}}=\boldsymbol{\tau_i}\cdot(\eta^n(\nabla\mathbf{u}^{n+\frac{1}{2}}+(\nabla\mathbf{u}^{n+\frac{1}{2}})^T)+\lambda^{n+\frac{1}{2}}\delta_\epsilon\mathcal{P}^n)\cdot\boldsymbol{n}, \quad (66)$$

$$-L^{n+\frac{1}{2}}\partial_{\tau_i}\phi^{n+\frac{1}{2}}\ ,\quad i=1,2, \quad (67)$$

We have the following derivations on those integration on the boundary.

$$\begin{aligned}
&\frac{\Delta t}{Re}\int_{\partial\Omega_w}\mathbf{u}^{n+\frac{1}{2}}\cdot\eta^n((\nabla\mathbf{u}^{n+\frac{1}{2}}+(\nabla\mathbf{u}^{n+\frac{1}{2}})^T)\cdot\boldsymbol{n})ds+\frac{\Delta t}{Re}\int_{\partial\Omega_w}\lambda^{n+\frac{1}{2}}(\delta_\epsilon\mathcal{P}^n\cdot\mathbf{n})\cdot\mathbf{u}_\tau^{n+\frac{1}{2}}ds\\
&+\frac{\mathcal{M}_s}{Re}\frac{S(\phi^{n+1})+S(\phi^n)-2S(\phi_0)}{2S(\phi_0)}\int_{\Omega_w}\varepsilon\partial_n\phi^{n+\frac{1}{2}}(\phi^{n+1}-phi^n)ds+\frac{\kappa_B}{Re}\int_{\Omega_w}\partial_n f^{n+\frac{1}{2}}(\phi^{n+1}-\phi^n)ds\\
&=\frac{\Delta t}{Re}\int_{\Omega_w}|\mathbf{u}_\tau^{n+\frac{1}{2}}|(-l_s^{-1}|\mathbf{u}_\tau^{n+\frac{1}{2}}|+L^{n+\frac{1}{2}}\partial_\tau\phi^{n+\frac{1}{2}})+\frac{1}{Re}\int_{\Omega_w}L^{n+\frac{1}{2}}(\phi^{n+1}-\phi^n)-\alpha_w(f_w^{n+1}-f_w^n)ds\\
&=-l_s^{-1}\frac{\Delta t}{Re}\int_{\Omega_w}|\mathbf{u}_\tau^{n+\frac{1}{2}}|^2ds+\frac{\Delta t}{Re}\int_{\Omega_w}L^{n+\frac{1}{2}}(\mathbf{u}_\tau^{n+\frac{1}{2}}\partial_\tau\phi^{n+\frac{1}{2}}+\frac{\phi^{n+1}-\phi^n}{\Delta t})ds+\alpha_w(||f_w^{n+1}||w-||f_w^n||_w)\\
&=\frac{\Delta t}{Re}(||-l_s^{-\frac{1}{2}}\mathbf{u}_\tau^{n+\frac{1}{2}}||w^2-\frac{1}{\kappa}||L^{n+\frac{1}{2}}||w^2)+\alpha_w(||f_w^{n+1}||w-||f_w^n||w) \quad (68)
\end{aligned}$$

By the definition of $\mathcal{E}_{kin}^n,\mathcal{E}_{cell}^n,\mathcal{E}_w^n$ and $\mathcal{E}_{kin}^{n+1},\mathcal{E}_{cell}^{n+1},\mathcal{E}_w^{n+1}$, we can finally get the energy law

$$\mathcal{E}_{total}^{n+1}-\mathcal{E}_{total}^n \quad = \quad (\mathcal{E}_{kin}^{n+1}+\mathcal{E}_{cell}^{n+1}+\mathcal{E}_w^{n+1})-(\mathcal{E}_{kin}^n+\mathcal{E}_{cell}^n+\mathcal{E}_w^n)$$

$$
\begin{aligned}
= \quad & \frac{\triangle t}{Re}\left(-2\|(\eta^n)^{1/2}\mathbf{D}_\eta^{n+\frac{1}{2}}\|^2 - \mathcal{M}\|\mu^{n+\frac{1}{2}}\|^2 - \xi\| \ \epsilon\phi^n\nabla\lambda^{n+\frac{1}{2}}\|^2\right. \\
& \left. -\frac{1}{\kappa}\|L(\phi^{n+\frac{1}{2}})\|_w^2 - \|l_s^{-1/2}\mathbf{u}_\tau^{n+\frac{1}{2}}\|_w^2\right) \ , \qquad (69)
\end{aligned}
$$

References

[1] Sebastian Aland et al. "Diffuse interface models of locally inextensible vesicles in a viscous fluid". In: *Journal of computational physics* 277 (2014), pp. 32–47.

[2] Joseph E Aslan et al. "Platelet shape change and spreading". In: *Platelets and Megakaryocytes*. Springer, 2012, pp. 91–100.

[3] Gilda A Barabino, Manu O Platt, and Dhananjay K Kaul. "Sickle cell biomechanics". In: *Annual review of biomedical engineering* 12 (2010), pp. 345–367.

[4] Himanish Basu et al. "Tank treading of optically trapped red blood cells in shear flow". In: *Biophysical journal* 101.7 (2011), pp. 1604–1612.

[5] Julien Beaucourt et al. "Steady to unsteady dynamics of a vesicle in a flow". In: *Physical Review E* 69.1 (2004), p. 011906.

[6] Thierry Biben, Klaus Kassner, and Chaouqi Misbah. "Phase-field approach to three-dimensional vesicle dynamics". In: *Physical Review E* 72.4 (2005), p. 041921.

[7] Andrea Bonito, Ricardo H Nochetto, and M Sebastian Pauletti. "Parametric FEM for geometric biomembranes". In: *Journal of Computational Physics* 229.9 (2010), pp. 3171–3188.

[8] Rui Chen et al. "Decoupled energy stable schemes for phase-field vesicle membrane model". In: *Journal of Computational Physics* 302 (2015), pp. 509–523.

[9] Rui Chen et al. "Decoupled energy stable schemes for phase-field vesicle membrane model". In: *Journal of Computational Physics* 302 (2015), pp. 509–523.

[10] Wenbin Chen et al. "Convergence analysis of a fully discrete finite difference scheme for the Cahn-Hilliard-Hele-Shaw equation". In: *Mathematics of Computation* 85.301 (2016), pp. 2231–2257.

[11] Kelong Cheng et al. "An energy stable fourth order finite difference scheme for the Cahn–Hilliard equation". In: *Journal of Computational and Applied Mathematics* 362 (2019), pp. 574–595.

[12] Philippe G Ciarlet. *Introduction to linear shell theory*. Vol. 98. Elsevier Masson, 1998.

[13] Amanda E Diegel and Shawn W Walker. " A Finite Element Method for a Phase Field Model of Nematic Liquid Crystal Droplets". In: *Communications in Computational Physics* 25 (2019), pp. 155–188.

[14] Qiang Du, Manlin Li, and Chun Liu. "Analysis of a phase field Navier-Stokes vesicle-fluid interaction model". In: *Discrete & Continuous Dynamical Systems-B* 8.3 (2007), p. 539.

[15] Qiang Du, Chun Liu, and Xiaoqiang Wang. "A phase field approach in the numerical study of the elastic bending energy for vesicle membranes". In: *Journal of Computational Physics* 198.2 (2004), pp. 450–468.

[16] Qiang Du and Jian Zhang. "Adaptive finite element method for a phase field bending elasticity model of vesicle membrane deformations". In: *SIAM Journal on Scientific Computing* 30.3 (2008), pp. 1634–1657.

[17] Qiang Du et al. "A phase field formulation of the Willmore problem". In: *Nonlinearity* 18.3 (2005), p. 1249.

[18] Qiang Du et al. "Modeling the spontaneous curvature effects in static cell membrane deformations by a phase field formulation". In: *Communications on Pure & Applied Analysis* 4.3 (2005), p. 537.

[19] Qiang Du et al. "Energetic variational approaches in modeling vesicle and fluid interactions". In: *Physica D: Nonlinear Phenomena* 238.9-10 (2009), pp. 923–930.

[20] Bob Eisenberg, Yunkyong Hyon, and Chun Liu. "Energy variational analysis of ions in water and channels: Field theory for primitive models of complex ionic fluids". In: *The Journal of Chemical Physics* 133.10 (2010), p. 104104.

[21] Thomas M Fischer. "Shape memory of human red blood cells". In: *Biophysical journal* 86.5 (2004), pp. 3304–3313.

[22] Caimi G and Presti RL. "Techniques to evaluate erythrocyte deformability in diabetes mellitus". In: *Acta Diabetol.* 41.3 (2004), pp. 99–103.

[23] Rui Gu, Xiaoqiang Wang, and M Gunzburger. "Simulating vesicle–substrate adhesion using two phase field functions". In: *Journal of Computational Physics* 275 (2014), pp. 626–641.

[24] Rui Gu, Xiaoqiang Wang, and Max Gunzburger. "A two phase field model for tracking vesicle–vesicle adhesion". In: *Journal of mathematical biology* 73.5 (2016), pp. 1293–1319.

[25] Francisco Guillén-González and Giordano Tierra. "Unconditionally energy stable numerical schemes for phase-field vesicle membrane model". In: *Journal of computational physics* 354 (2018), pp. 67–85.

[26] Z. Guo et al. "Mass conservative and energy stable finite difference methods for the quasi-incompressible Navier-Stokes-Cahn-Hilliard system: Primitive variable and projection-type schemes". In: *Computer Methods in Applied Mechanics and Engineering* 326 (Nov. 2017), pp. 144–174. ISSN: 0045-7825. DOI: 10.1016/j.cma.2017.08.011.

[27] Zhenlin Guo and Ping Lin. "A thermodynamically consistent phase-field model for two-phase flows with thermocapillary effects". In: *Journal of Fluid Mechanics* 766 (2015), pp. 226–271.

[28] Zhenlin Guo, Ping Lin, and John S Lowengrub. "A numerical method for the quasi-incompressible Cahn–Hilliard–Navier–Stokes equations for variable density flows with a discrete energy law". In: *Journal of Computational Physics* 276 (2014), pp. 486–507.

[29] Yunlong Han et al. "Flow-induced translocation of vesicles through a narrow pore". In: *Soft matter* 15.16 (2019), pp. 3307–3314.

[30] Wenrui Hao et al. "A fictitious domain method with a hybrid cell model for simulating motion of cells in fluid flow". In: *Journal of Computational Physics* 280 (2015), pp. 345–362.

[31] Dan Hu, Pingwen Zhang, and E Weinan. "Continuum theory of a moving membrane". In: *Physical Review E* 75.4 (2007), p. 041605.

[32] Wei-Fan Hu et al. "Vesicle electrohydrodynamic simulations by coupling immersed boundary and immersed interface method". In: *Journal of Computational Physics* 317 (2016), pp. 66–81.

[33] Jinsong Hua et al. "Energy law preserving C0 finite element schemes for phase field models in two-phase flow computations". In: *Journal of Computational Physics* 230.19 (2011), pp. 7115–7131.

[34] George Barker Jeffery. "The motion of ellipsoidal particles immersed in a viscous fluid". In: *Proceedings of the Royal Society of London. Series A, Containing papers of a mathematical and physical character* 102.715 (1922), pp. 161–179.

[35] James T Jenkins. "The equations of mechanical equilibrium of a model membrane". In: *SIAM Journal on Applied Mathematics* 32.4 (1977), pp. 755–764.

[36] Yongsam Kim and Ming-Chih Lai. "Simulating the dynamics of inextensible vesicles by the penalty immersed boundary method". In: *Journal of Computational Physics* 229.12 (2010), pp. 4840–4853.

[37] Ebrahim M Kolahdouz and David Salac. "A numerical model for the trans-membrane voltage of vesicles". In: *Applied Mathematics Letters* 39 (2015), pp. 7–12.

[38] Aymen Laadhari, Pierre Saramito, and Chaouqi Misbah. "Vesicle tumbling inhibited by inertia". In: *Physics of Fluids* 24.3 (2012), p. 031901.

[39] Zhen Li et al. "A dissipative particle dynamics method for arbitrarily complex geometries". In: *Journal of Computational Physics* 355 (2018), pp. 534–547.

[40] Ping Lin and Chun Liu. "Simulations of singularity dynamics in liquid crystal flows: A C0 finite element approach". In: *Journal of Computational Physics* 215.1 (2006), pp. 348–362.

[41] Kai Liu et al. "Dynamics of a multicomponent vesicle in shear flow". In: *Soft matter* 13.19 (2017), pp. 3521–3531.

[42] John S Lowengrub, Andreas Rätz, and Axel Voigt. "Phase-field modeling of the dynamics of multicomponent vesicles: Spinodal decomposition, coarsening, budding, and fission". In: *Physical Review E* 79.3 (2009), p. 031926.

[43] Roy Malka, David M Nathan, and John M Higgins. "Mechanistic modeling of hemoglobin glycation and red blood cell kinetics enables personalized diabetes monitoring". In: *Science translational medicine* 8.359 (2016), 359ra130–359ra130.

[44] Wieland Marth, Sebastian Aland, and Axel Voigt. "Margination of white blood cells: a computational approach by a hydrodynamic phase field model". In: *Journal of Fluid Mechanics* 790 (2016), pp. 389–406.

[45] Arman Namvar et al. "Surface area-to-volume ratio, not cellular viscoelasticity, is the major determinant of red blood cell traversal through small channels". In: *Cellular Microbiology* (2020), e13270.

[46] Hiroshi Noguchi and Gerhard Gompper. "Shape transitions of fluid vesicles and red blood cells in capillary flows". In: *Proceedings of the National Academy of Sciences* 102.40 (2005), pp. 14159–14164. ISSN: 0027-8424. DOI: 10.1073/pnas.0504243102. eprint: https://www.pnas.org/content/102/40/14159.full.pdf. URL: https://www.pnas.org/content/102/40/14159.

[47] Kian Chuan Ong and Ming-Chih Lai. "An immersed boundary projection method for simulating the inextensible vesicle dynamics". In: *Journal of Computational Physics* 408 (2020), p. 109277.

[48] Igor V Pivkin and George Em Karniadakis. "Accurate coarse-grained modeling of red blood cells". In: *Physical review letters* 101.11 (2008), p. 118105.

[49] Igor V Pivkin, Peter D Richardson, and George Em Karniadakis. "Effect of red blood cells on platelet aggregation". In: *IEEE Engineering in Medicine and Biology Magazine* 28.2 (2009), pp. 32–37.

[50] J. Pöschl et al. "Endotoxin binding to erythrocyte membrane and erythrocyte deformability in human sepsis and in vitro". In: *Critical Care Medicine* 31 (2003), pp. 924–928.

[51] Tiezheng Qian, Xiao-Ping Wang, and Ping Sheng. "A variational approach to moving contact line hydrodynamics". en. In: *Journal of Fluid Mechanics* 564 (Oct. 2006), p. 333. ISSN: 0022-1120, 1469-7645. DOI: 10.1017/S0022112006001935.

[52] Tiezheng Qian, Xiao-Ping Wang, and Ping Sheng. "A variational approach to the moving contact line hydrodynamics". In: *arXiv preprint cond-mat/0602293* (2006).

[53] Tiezheng Qian, Xiao-Ping Wang, and Ping Sheng. "Molecular hydrodynamics of the moving contact line in two-phase immersible flows". In: *Commun. Comput. Phys.* (2006), p. 52.

[54] Yuzhe Qin et al. "A phase field model for mass transport with semi-permeable interfaces". In: *arXiv preprint arXiv:2103.06430* (2021).

[55] Weiqing Ren and Weinan E. "Heterogeneous multiscale method for the modeling of complex fluids and micro-fluidics". In: *Journal of Computational Physics* 204.1 (Mar. 2005), pp. 1–26. ISSN: 00219991. DOI: 10.1016/j.jcp.2004.10.001.

[56] Weiqing Ren and Weinan E. "Boundary conditions for the moving contact line problem". In: *Physics of fluids* 19.2 (2007), p. 022101.

[57] Céline Renoux et al. "Impact of surface-area-to-volume ratio, internal viscosity and membrane viscoelasticity on red blood cell deformability measured in isotonic condition". In: *Scientific reports* 9.1 (2019), pp. 1–7.

[58] David Salac and Michael Miksis. "A level set projection model of lipid vesicles in general flows". In: *Journal of Computational Physics* 230.22 (2011), pp. 8192–8215.

[59] Nicholas J Savill and Paulien Hogeweg. "Modelling morphogenesis: from single cells to crawling slugs". In: *Journal of theoretical biology* 184.3 (1997), pp. 229–235.

[60] Yunchang Seol et al. "An immersed boundary method for simulating vesicle dynamics in three dimensions". In: *Journal of Computational Physics* 322 (2016), pp. 125–141.

[61] Lingyue Shen et al. "An energy stable C0 finite element scheme for a quasi-incompressible phase-field model of moving contact line with variable density". In: *Journal of Computational Physics* 405 (2020), p. 109179.

[62] Eun-Kyung Shin et al. "Platelet shape changes and cytoskeleton dynamics as novel therapeutic targets for anti-thrombotic drugs". In: *Biomolecules & therapeutics* 25.3 (2017), p. 223.

[63] Shu Takagi et al. "The deformation of a vesicle in a linear shear flow". In: *Journal of applied mechanics* 76.2 (2009).

[64] Naoki Takeishi et al. "Deformation of a Red Blood Cell in a Narrow Rectangular Microchannel". In: *Micromachines* 10.3 (2019), p. 199.

[65] Xiaolong Wang et al. "An immersed boundary method for mass transfer through porous biomembranes under large deformations". In: *Journal of Computational Physics* (2020), p. 109444.

[66] Steven M Wise, Cheng Wang, and John S Lowengrub. "An energy-stable and convergent finite-difference scheme for the phase field crystal equation". In: *SIAM Journal on Numerical Analysis* 47.3 (2009), pp. 2269–2288.

[67] Hao Wu and Xiang Xu. "Strong solutions, global regularity, and stability of a hydrodynamic system modeling vesicle and fluid interactions". In: *SIAM Journal on Mathematical Analysis* 45.1 (2013), pp. 181–214.

[68] Tenghu Wu and James J Feng. "Simulation of malaria-infected red blood cells in microfluidic channels: Passage and blockage". In: *Biomicrofluidics* 7.4 (2013), p. 044115.

[69] Jian-Jun Xu and Weiqing Ren. "A level-set method for two-phase flows with moving contact line and insoluble surfactant". In: *Journal of Computational Physics* 263 (Apr. 2014), pp. 71–90. ISSN: 0021-9991. DOI: 10.1016/j.jcp.2014.01.012.

[70] Jian-Jun Xu et al. "A level-set method for interfacial flows with surfactant". en. In: *Journal of Computational Physics* 212.2 (Mar. 2006), pp. 590–616. ISSN: 00219991. DOI: 10.1016/j.jcp.2005.07.016.

[71] Shixin Xu, Mark Alber, and Zhiliang Xu. "Three-phase Model of Visco-elastic Incompressible Fluid Flow and its Computational Implementation". In: *Communications in Computational Physics.* 25(2) (2019), pp. 586–624.

[72] Shixin Xu, Ping Sheng, and Chun Liu. "An energetic variational approach for ion transport". In: *Communications in Mathematical Sciences* 12.4 (2014), pp. 779–789.

[73] Shixin Xu et al. "Model predictions of deformation, embolization and permeability of partially obstructive blood clots under variable shear flow". In: *Journal of the Royal Society, Interface* 14.136 (2017). ISSN: 1742-5662. DOI: 10.1098/rsif.2017.0441.

[74] Shixin Xu et al. "Osmosis through a semi-permeable membrane: a consistent approach to interactions". In: *arXiv preprint arXiv:1806.00646* (2018).

[75] Zhiliang Xu et al. "A multiscale model of thrombus development". In: *Journal of the Royal Society Interface* 5.24 (2008), pp. 705–722.

[76] Yue Yan et al. "A second-order energy stable BDF numerical scheme for the Cahn-Hilliard equation". In: *Commun. Comput. Phys.* 23.2 (2018), pp. 572–602.

[77] Xiaofeng Yang and Guo-Dong Zhang. "Convergence Analysis for the Invariant Energy Quadratization (IEQ) Schemes for Solving the Cahn–Hilliard and Allen–Cahn Equations with General Nonlinear Potential". In: *Journal of Scientific Computing* 82.3 (2020), pp. 1–28.

[78] Xiaofeng Yang, Jia Zhao, and Qi Wang. "Numerical approximations for the molecular beam epitaxial growth model based on the invariant energy quadratization method". In: *Journal of Computational Physics* 333 (2017), pp. 104–127.

[79] Xiaofeng Yang et al. "Numerical approximations for a three-component Cahn–Hilliard phase-field model based on the invariant energy quadratization method". In: *Mathematical Models and Methods in Applied Sciences* 27.11 (2017), pp. 1993–2030.

[80] Jian Zhang, Sovan Das, and Qiang Du. "A phase field model for vesicle–substrate adhesion". In: *Journal of Computational Physics* 228.20 (2009), pp. 7837–7849.